This document is confidential and is proprietary to the American Chemical Society and its authors. Do not copy or disclose without written permission. If you have received this item in error, notify the sender and delete all copies.

Probing the Chemical Bond Between Lanthanides and Carbon: CeC, PrC, NdC, LuC, and TmC₂

Journal:	Inorganic Chemistry
Manuscript ID	ic-2023-01042n.R2
Manuscript Type:	Article
Date Submitted by the Author:	12-May-2023
Complete List of Authors:	Merriles, Dakota; University of Utah, Department of Chemistry London, Anthony; University of Utah, Department of Chemistry Tieu, Erick; University of Utah, Department of Chemistry Nielson, Christopher; University of Utah, Department of Chemistry Morse, Michael; University of Utah, Department of Chemistry

SCHOLARONE™ Manuscripts Probing the Chemical Bond Between Lanthanides and Carbon: CeC, PrC, NdC, LuC, and TmC2

Dakota M. Merriles, Anthony London, Erick Tieu, Christopher Nielson, and Michael D. Morse*

Department of Chemistry

University of Utah

Salt Lake City, Utah 84112

^{*}Author to whom correspondence should be addressed: morse@chem.utah.edu

ABSTRACT

Resonant two-photon ionization experiments have been conducted to probe the bond dissociation energy (BDE) of the lanthanide-carbon bond, allowing the BDEs of CeC, PrC, NdC, LuC, and Tm-C₂ to be measured to high precision. Values of $D_0(CeC) = 4.893(3) \text{ eV}$, $D_0(PrC) = 4.052(3) \text{ eV}$, $D_0(NdC) = 3.596(3) \text{ eV}, D_0(LuC) = 3.685(4) \text{ eV}, \text{ and } D_0(Tm-C_2) = 4.797(6) \text{ eV}$ are obtained. Additionally, the adiabatic ionization energy of LuC was measured, giving IE(LuC) = 7.05(3) eV. The electronic structure of these species, along with the previously measured LaC, has been further investigated using quantum chemical calculations. Despite LaC, CeC, PrC, and NdC having ground electronic configurations that differ only in the number of 4f electrons present, and have virtually identical bond orders, bond lengths, fundamental stretching frequencies, and metallic oxidation states, a peculiar 1.30 eV range in bond dissociation energies exists for these molecules. A natural bond orbital analysis shows that the metal atoms in these molecules have a natural charge of +1 with a 5d² 4f^h 6s⁰ configuration while the carbon atom has a natural charge of -1 and a 2p³ configuration. The diabatic bond dissociation energies, calculated with respect to the lowest energy level of this separated ion configuration, show a greatly reduced energy range of 0.32 eV, with the diabatic BDE decreasing as the amount of 4f character in the σ -bond increases. Thus, the wide range of measured BDEs for these molecules is a consequence of the variation in atomic promotion energies at the separated ion limit. TmC₂ has a smaller bond dissociation energy than the other LnC₂ molecules, due to the tiny amount of 5d participation in the valence molecular orbitals.

I. INTRODUCTION

The nature of the chemical bond between metal atoms and carbon, along with the chemistry of species containing the metal-carbon bond, are of primary interest to inorganic and organometallic chemists. It has been established for well over a century that transition metal-based organometallic compounds participate in an array of fascinating reactions and have many relevant applications.^{1, 2} However, perspectives regarding organometallic complexes incorporating lanthanide metals have undergone a major transformation in the last 50 years. In 1971, Pimentel and Spratley described the chemistry of the lanthanides,³ writing that "Lanthanum has only one important oxidation state in aqueous solution, the +3 state. With few exceptions, this tells the whole boring story about the other lanthanides." Since then, it has been well-documented that organometallic complexes containing lanthanides can participate in interesting and exotic chemistries and have the ability to access several oxidation states.⁴⁻¹⁰ Accordingly, numerous organolanthanide compounds have been studied and characterized using a variety of experimental and computational methodologies.¹¹⁻²⁵ The bonding schemes between the lanthanide atoms and carbon in these compounds are quite diverse, featuring single and multiple lanthanide-carbon bonds and well-characterized σ-, π-, and backbonding interactions.

Conversely, a paucity of reports exists in the literature for the simplest organolanthanide compound and the most fundamental lanthanide-carbon bond: the diatomic lanthanide carbide (LnC) molecules. In fact, it has been noted that even the production of lanthanide monocarbide molecules, much less their spectroscopic study, has remained elusive. ^{26,27} To the best of our knowledge, only two neutral lanthanide monocarbides have been previously studied by experimental methods: the bond dissociation energy (BDE) of LaC and CeC has been measured using Knudsen effusion mass spectrometry, ²⁸⁻³¹ and the BDE of LaC has been measured in our group using resonant two-photon ionization (R2PI) spectroscopy. ³² In the present work, we demonstrate the synthesis and accurate measurement of the bond dissociation energy *via* the observation of a sharp predissociation threshold in the resonant two-photon ionization spectra of CeC, PrC, NdC, LuC, and TmC₂. The diatomic CeC, PrC, NdC, and LuC molecules are the smallest species containing the lanthanide-carbon bond that can be studied, and therefore, present

excellent opportunities for understanding the fundamental nature of the lanthanide-carbon bond. Moreover, Ce, Pr, Nd, and Lu all have different electronic occupancies of the 5*d*- and 4*f*-orbitals in their atomic ground states, which presents the potential for a variety of bonding schemes in this family of diatomic molecules. Detailing the chemical bonding and electronic structure of this previously unstudied family of LnC species will assist in developing an intuition of the bonding behavior of the LnC species, providing quantitative and qualitative bonding trends of these molecules, and giving valuable spectroscopically derived thermochemical data for the refinement of computational methods for the lanthanides.

Accurate measurements of the BDEs of these molecules provide stringent benchmarks for newly emerging quantum chemical methodologies that aim to better predict the chemical properties of lanthanide containing compounds. 33-38 The currently available thermochemical data for lanthanide-containing compounds is scarce in quantity and has large error limits; in some cases it has been obtained purely on the basis of previously defined trends. 39 These limitations on the currently available data have led to the adoption of a 5 kcal/mol standard for achieving "experimental accuracy" in computations on lanthanide species, 40 a greatly relaxed standard for experimental accuracy than the 1 kcal/mol standard first proposed by Pople for main-group compounds. 41 The BDEs of the neutral LnC and TmC2 molecules reported here readily meet Pople's 1 kcal/mol standard in their precision and accuracy and can also be employed in various thermochemical cycles to extract additional pertinent thermochemical information that can be further used for understanding chemical trends and as quantitative benchmarks. A particularly useful thermochemical cycle relates the BDE of the neutral LnC molecule, the ionization energy (IE) of the Ln atom, the IE of the neutral LnC molecule, and the BDE of the cationic LnC+ via

$$D_0(LnC) + IE(Ln) = IE(LnC) + D_0(Ln^+-C).$$
 (1.1)

An analogous and equally useful thermochemical cycle relates the electron affinity (EA) of the neutral LnC, the BDE of the neutral LnC, the BDE of the anionic LnC molecule, and the EA of the C atom:

$$EA(LnC) + D_0(LnC) = D_0(Ln-C^-) + EA(C).$$
 (1.2)

A thermochemical cycle analogous to (1.1) relates the four quantities D₀(LnC), IE(C), IE(LnC) and D₀(Ln-C⁺); similarly, a cycle analogous to (1.2) relates the quantities EA(LnC), D₀(LnC), D₀(Ln-C), and EA(Ln). The ionization energies and electron affinities of the atoms, for the most part, are well known and are tabulated.^{42, 43} However, thermochemical values for neutral, cationic, and anionic LnC molecules are mostly absent from the current literature, in contrast to what is available for their transition metal and main-group counterparts. The spectroscopically measured BDEs for CeC, PrC, NdC, and LuC and the IE for LuC reported in this work can contribute to the completion of the thermochemical cycles listed above and be used to extract additional information on these molecules when they are inserted into Eqns. 1.1 and 1.2.

Very recently, there has been a reexamination of the role that the 4f orbitals play in the bonding and electronic structure of molecules that contain lanthanide elements. The conventional notion that the radially contracted and "core-like" 4f-electrons do not participate in bonding, or at least do so to a substantially lesser degree than do the 5f-electrons of the actinides, 44, 45 has been widely accepted. Recent evidence suggests, however, that the 4f orbitals of the lanthanides can participate in bonding in some lanthanide containing molecules. 46 The solid LnO₂ compounds (Ln = Ce, Pr, Tb) have been investigated via X-ray absorption spectroscopy, for example, and considerable orbital mixing between the Ln 4f orbitals and the oxygen 2p orbitals in both σ - and π -type interactions has been found.⁴⁷ An X-ray absorption spectroscopy study on $LnCl_6^{-x}$ (Ln = Ce, Nd, Sm, Eu, Gd; x = 2, 3) compounds showed that upon oxidizing Ce(III) to Ce(IV), Ce 4f and Cl 3p mixing is markedly increased, with the 4f-3p mixing being more than double that observed for the 5f-3p mixing in the UCl₆-2 anion. 48 In a study of La-based endohedral metallofullerenes (EMFs), the La 4f-orbitals are found to play a critical role in the chemical reactivity and structure of the EMFs, with the La 4f-orbitals becoming more important as the size of the carbon cage is reduced.⁴⁹ Reactions between Ce and acetonitrile studied by matrix infrared spectroscopy in neon matrices and density functional theory calculations reveal that the 4f-orbitals of Ce become active and participate in the bonding between Ce and C and N in Ce-n²-(NC)-CH₃ π -complexes.⁵⁰ In addition to the brief overview of the literature above, there is a plethora of other recent examples where 4f-orbitals

have been found to play an important role in lanthanide containing compounds.⁵¹⁻⁵⁶ It is of current interest to add to this developing field by probing small Ln containing molecules, like the diatomic lanthanide carbides, to further investigate the contributions of the 4f orbitals to the chemical bond. Thulium dicarbide, TmC₂, for example, is a triatomic lanthanide carbide system where the lanthanide atom has a large energy gap (1.63 eV) between its 6s²4f¹³ ground atomic configuration and its first excited 6s²5d¹4f¹² atomic configuration.⁴² The high energy required to access the 5d orbitals of thulium may force TmC₂ to use the 4*f* orbitals to form chemical bonds.

II. METHODS

A. Experimental Methods

The instrument used to measure the predissociation thresholds of CeC, PrC, NdC, LuC, and TmC₂ using R2PI spectroscopy is the same as that used to study the BDEs of various LnS and LnSe molecules.⁵⁷ To begin, the instrument is separated into two chambers, termed the source chamber and analytical chamber, which are evacuated to 10⁻⁵ Torr and 10⁻⁶ Torr, respectively. The LnC and LnC₂ molecules of interest are produced in a laser ablation source situated inside the source chamber. The source consists of a stainless-steel reaction block with two perpendicular, intersecting channels. One channel, termed the reaction channel, terminates in the source chamber via an exit orifice. At the opposite end of the reaction channel is a pulsed nozzle that supplies gas to the reaction channel. In these experiments, the pulsed nozzle admits a high-pressure (~10-20 psig) pulse of helium seeded with 4% methane, flooding the reaction channel. For production of TmC2, 1% acetylene seeded in helium was used. Immediately after the pulse of gas is triggered, a pulse of focused laser light (532 nm) from a pulsed Nd:YAG laser irradiates the surface of a metal lanthanide disk (1 in. square × 1 mm thick) held flush to the end of a channel perpendicular to the reaction channel. When this intense, focused light strikes the metal surface, a plasma of lanthanide atoms, ions, and electrons is ejected into the gas phase. The plasma is entrained into the reaction channel, where chemical reactions between the constituents of the plasma and the reactive methane/acetylene molecules commence. The products of these reactions, the lanthanide

carbide molecules of interest, travel down the reaction channel toward the exit orifice. During their travel down the reaction channel, the molecules undergo numerous collisions in this high-pressure environment with helium atoms, cooling the lanthanide carbide molecules to near ambient temperatures.

When the reaction products exit the reaction channel, they undergo a supersonic expansion as they enter the low-pressure (~10-5 Torr) source chamber. The supersonic expansion cools the rotational temperature of the molecules to less than 30 K.58 The expansion eventually reaches a conical skimmer with a 1 cm orifice, which admits a loosely collimated molecular beam into the analytical chamber. The molecular beam continues travelling forward, reaching the center of a Wiley-McLaren electrode assembly mounted inside the chamber. This is where the molecules are ionized.

In the center of the Wiley-McLaren electrode assembly, the molecular beam is irradiated with photons emitted by a tunable optical parametric oscillator (OPO) laser that counterpropagates along the molecular beam axis. If the energy of these photons is resonant with a spectroscopic transition, the molecules are promoted into the excited state. In almost all our previous R2PI experiments, 32, 60, 61 the excited molecules are then irradiated by high-energy photons produced by a second, perpendicularly oriented ionization laser. In the experiments for CeC, PrC, NdC, and LuC, however, the molecules were ionized by absorption of a second photon from the same OPO laser pulse that initially excited them. This was possible because the excitation energies used in these experiments were greater than half the ionization energies of the LnC molecules, allowing a one-color two-photon ionization scheme to be realized. The same ionization scheme was also used in our measurements of the ionization energies of the late transition metal borides. 62 Regardless, as soon as the constituents of the molecular beam are ionized, they are accelerated upward into the time-of-flight mass spectrometer. The newborn ions continue traveling upward through a drift tube, traverse a reflectron apparatus, and then impact a dual microchannel plate (MCP) detector at different times, dependent on the mass of the ion. Ultimately, the temporal resolution afforded by the MCP detector and the spectroscopic resolution of the OPO laser allows mass-resolved optical spectra to be recorded and monitored for multiple species in a single R2PI spectroscopy experiment.

The trigger timings that control the pulsing of the gas nozzle, the firing of each laser, and the electronics of the MCP detector are based on a master oscillator operating at 10 Hz. In other words, 10 experimental cycles, beginning with the production of the LnC molecules of interest and ending with the digitization of ions impacting the MCP detector, occur per second. For the spectroscopic investigations employed to measure the predissociation thresholds of the lanthanide carbides, 30 experimental cycles are recorded at every 0.05 nm incremental step as the OPO laser is scanned through a predefined set of wavelengths. Once the predissociation threshold has been located for a molecule, an averaged spectrum and acceptable signal-to-noise ratio is obtained by repeating the same scan at least three times over the energy range that spans the predissociation threshold. After the averaged spectrum is obtained, the spectrum is calibrated to atomic transitions from NIST.⁴² The atomic transitions are collected either by recording the lanthanide atomic signal simultaneously with the predissociation threshold, or if no identifiable lanthanide atomic transitions are found, then a different metal sample is installed in order to record atomic spectra that can be used for calibration.

B. Computational Methods

The Gaussian16 software package was used for all quantum chemical calculations in this work.⁶³
The geometries of CeC, PrC, NdC, and LuC were optimized with various spin multiplicities to determine the ground electronic configuration and spin for each LnC species. For CeC, singlet, triplet, quintet, and septet spin multiplicities were used. For PrC and LuC, doublet, quartet, sextet, and octet spin multiplicities were used. For NdC, triplet, quintet, septet, and nonet spin multiplicities were used. For these geometry optimizations, the unrestricted B3LYP density functional was employed.⁶⁴ The lanthanide constituents in each molecule were calculated with an all-electron correlation consistent basis set of triplezeta quality, cc-pVTZ-DK3.⁶⁵ For the C atom, the related all-electron aug-cc-pVTZ-DK basis set was used in the geometry optimization calculations.⁶⁶⁻⁶⁸ In the calculations involving the -DK3/-DK basis sets, a Douglas-Kroll-Hess 2nd order scalar relativistic calculation was employed (Keyword:

Integral=DKH2).⁶⁹⁻⁷¹ Once the global minimum geometries and ground electronic states of CeC, PrC,

NdC, and LuC were found, calculations with coupled-cluster single double perturbative triple (CCSD(T))

theory were performed on each molecule using the global minimum geometries and molecular orbital occupancies found in the geometry optimizations to obtain single-point energies for each molecule. The CCSD(T) theory single-point calculations were performed with the cc-pVTZ-DK3 basis sets for the Ln atom and the aug-cc-pVTZ-DK basis set for the C atom.

TmC₂ is a triatomic molecule and naturally has a range of possible isomers for its global minimum geometry. Following the same procedure for our recent work on triatomic MB₂ species, 72 TmC₂ had its global minimum geometry calculated with doublet, quartet, sextet, and octet spin multiplicities and three different chemically reasonable structural isomers: (1) a triangular, cyclic C_{2v} geometry, (2) a linear geometry where the two carbon atoms are bonded end-on to the Tm atom (Tm-C-C), and (3) a linear geometry where the Tm atom is intercalated between the two carbon atoms (C-Tm-C). All of the geometry optimizations for the elucidation of the TmC₂ global minimum and ground electronic configuration were performed using the unrestricted B3LYP density functional. ⁶⁴ The Tm atom was calculated with the polarized valence quadruple-zeta quality Stuttgart RSC ANO basis set^{73, 74} and its corresponding relativistic small-core effective core potential while the carbon atoms were calculated with the all-electron aug-cc-pVQZ basis set. ^{67, 68} The global minimum geometry for TmC₂ was unambiguously found to be the cyclic C_{2v} geometry. After this geometry confirmation, single-point CCSD(T) calculations were carried out with the same basis sets, molecular orbital occupancies, and geometries found from the TmC₂ geometry optimization. All basis sets were obtained from the Basis Set Exchange. ⁷⁵

III. RESULTS

Figures 1-4 display the R2PI spectra and predissociation thresholds of CeC, PrC, NdC, and LuC, respectively. In these spectra, the top blue trace is the molecular signal of the lanthanide carbide of

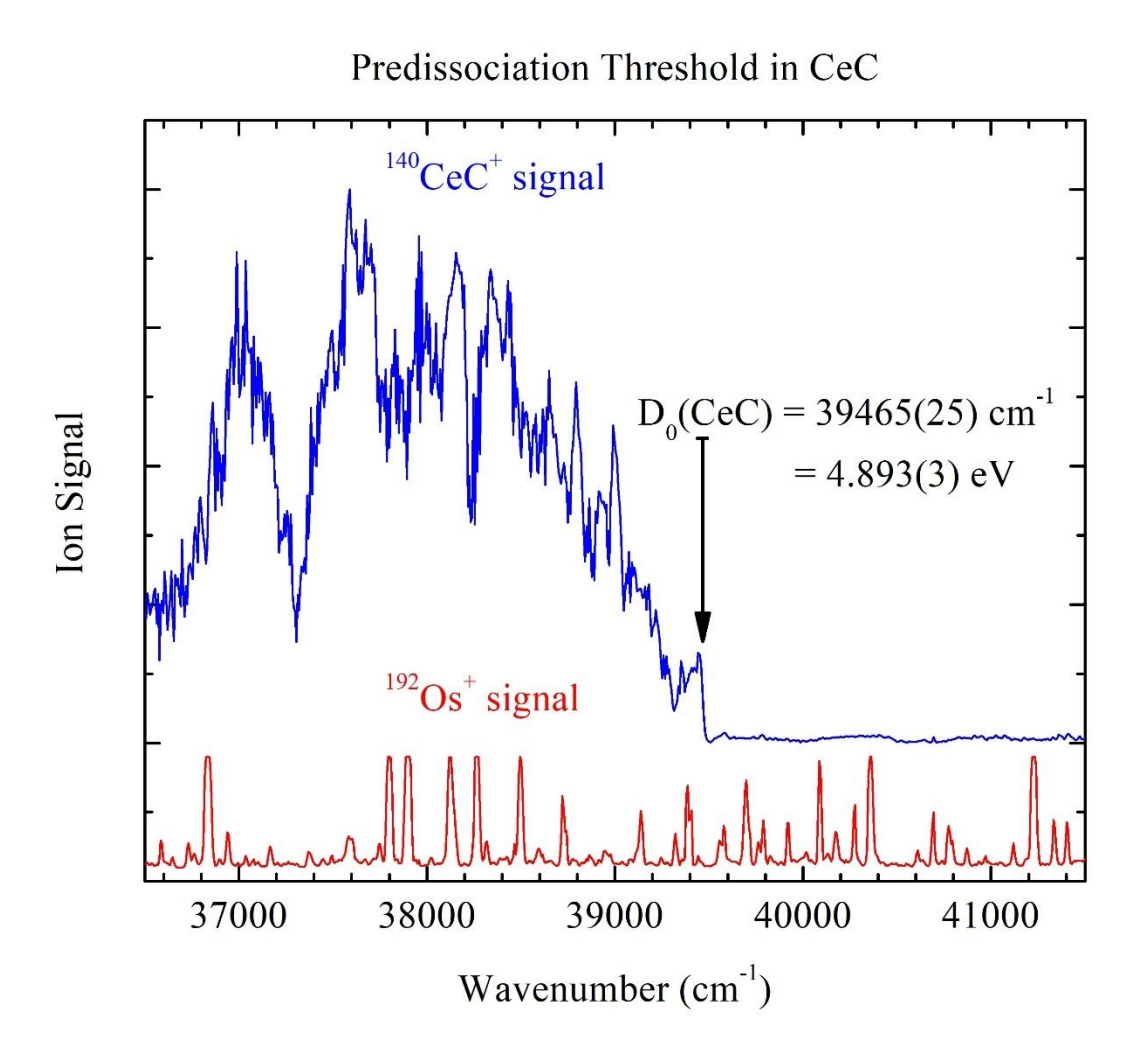


Figure 1. R2PI spectrum of CeC (upper, blue trace) with its predissociation threshold at 39 465(25) cm⁻¹.

The atomic spectrum of Os (bottom, red trace) was used for calibration.

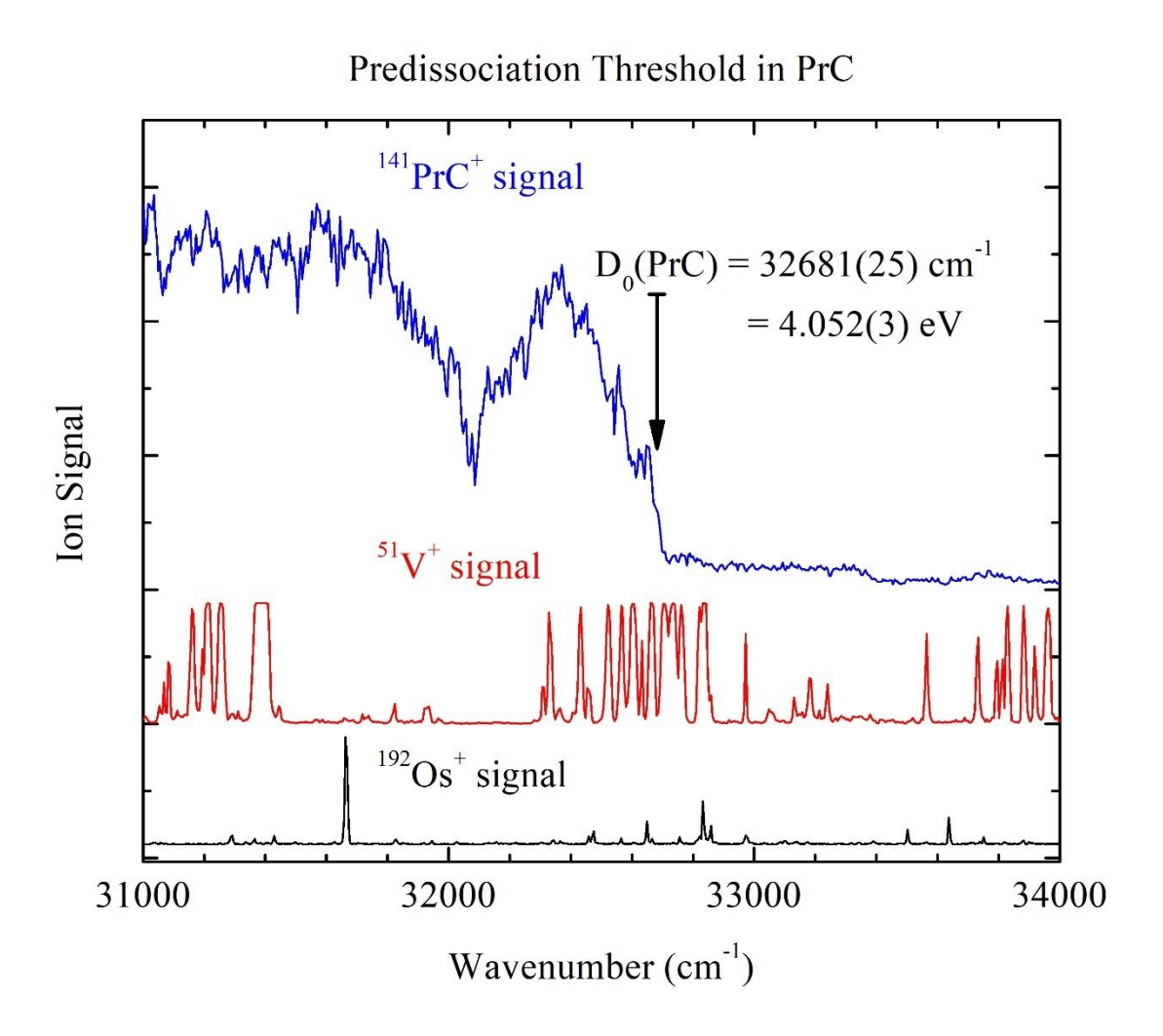


Figure 2. R2PI spectrum of PrC (upper, blue trace) with its predissociation threshold at 32 681(25) cm⁻¹.

The atomic spectra of V (center, red trace) and Os (bottom, black trace) were used for calibration.

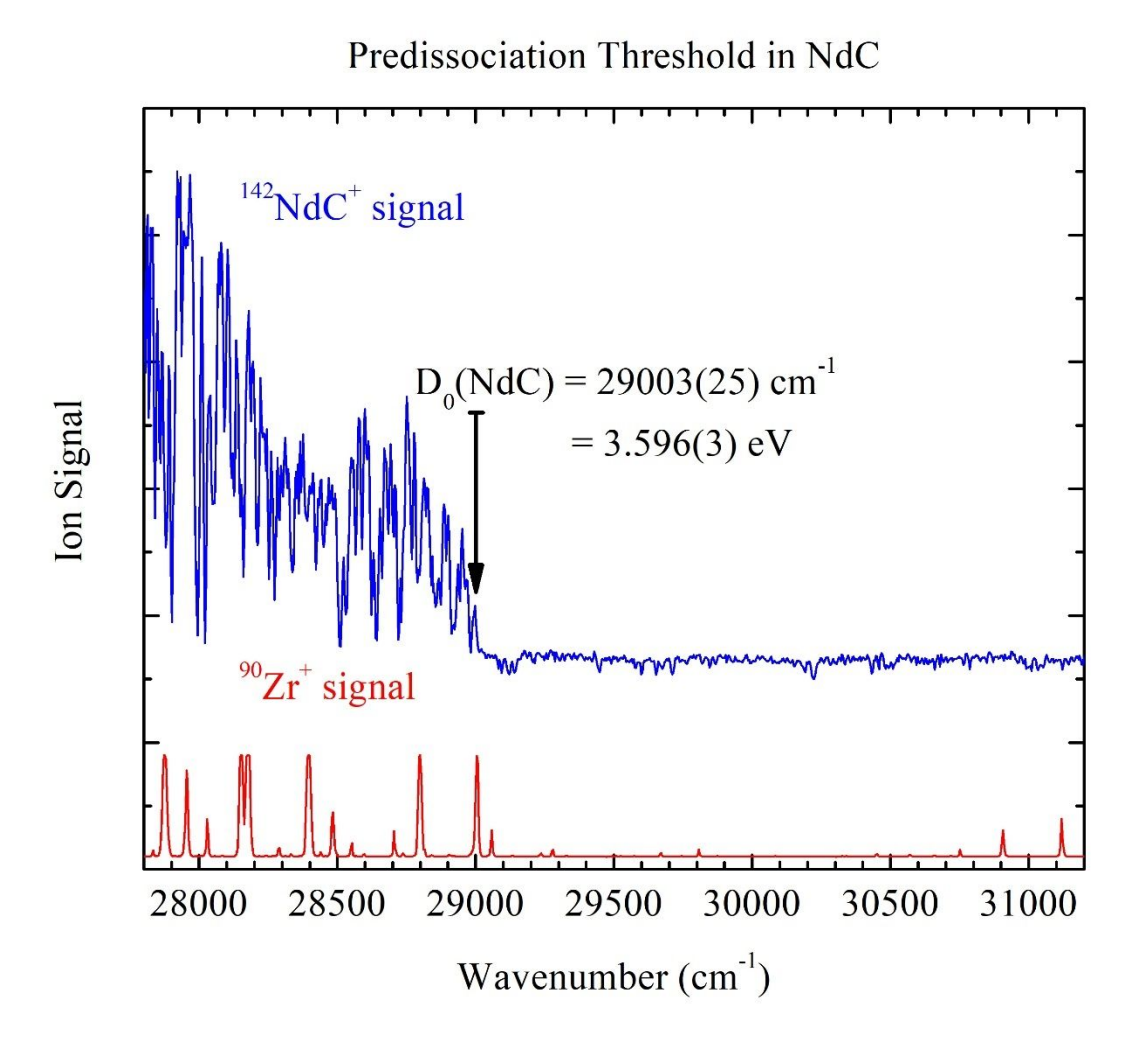


Figure 3. R2PI spectrum of NdC (upper, blue trace) with its predissociation threshold at 29 003(25) cm⁻¹.

The atomic spectrum of Zr (lower, red trace) was used for calibration.

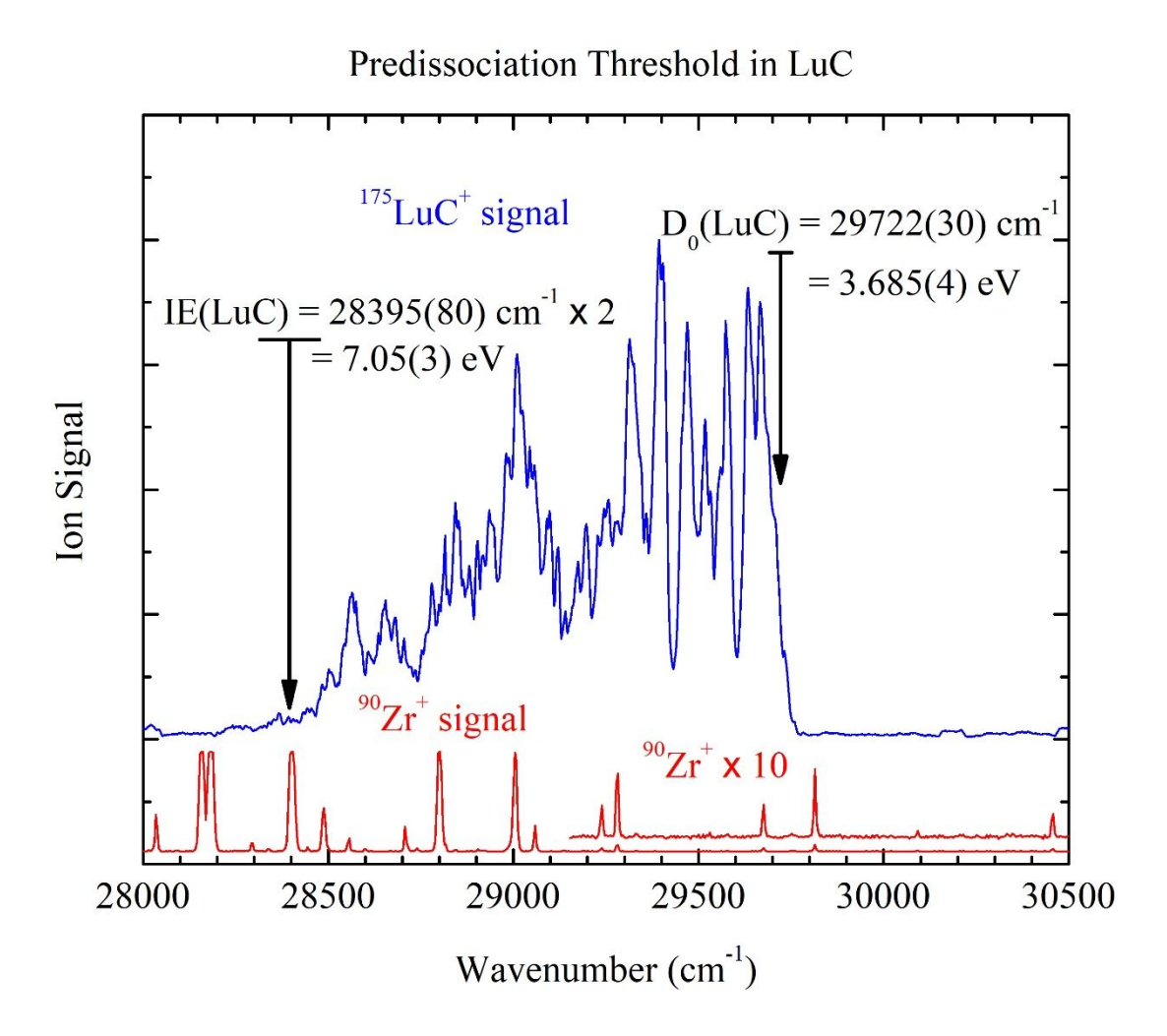


Figure 4. R2PI spectrum of LuC (top, blue trace) with its predissociation threshold at 29 722(30) cm⁻¹ and its two-photon ionization threshold at 28 395(80) cm⁻¹. The atomic spectrum of Zr (lower, red trace) was used for calibration. Above 29 100 cm⁻¹, the Zr atomic signal is magnified ten-fold to better show the less intense Zr atomic transitions.

interest. Below the top trace are the recorded atomic signal(s) that were used for calibration. The predissociation threshold for each LnC molecule is readily identified by a visual cue: an abrupt decrease in ion signal from that of a convoluted, quasi-continuous vibronic spectrum below the threshold to a baseline of nominally zero ion signal. The abrupt drop in ion signal occurs because spin-orbit and nonadiabatic couplings among the multitude of electronic states in this energetic region allow the molecule to hop from one potential curve to another quite readily, rapidly finding its way to separated ground state atoms as soon as the bond dissociation energy is exceeded. 76, 77 This process happens so rapidly that the molecule dissociates into its ground state atomic fragments before it can absorb a second photon and be ionized. Thus, the ion signal disappears when the molecule is excited to states at or above its ground separated atom limit. The use of spectroscopically measured predissociation thresholds to assign accurate BDEs to molecules with high electronic state densities has long been employed and discussed by our group. 61, 78-81 The argument that sharp predissociation thresholds may be identified with thermochemical BDEs is strengthened by thermochemical cycles that demonstrate exceptional self-consistency when BDE values obtained from predissociation thresholds are employed in these cycles. 32, 79

In each spectrum, the assigned predissociation threshold is indicated by an arrow. Atop the arrow is a black horizontal bar, spanning the energy range corresponding to the error limit assigned to the BDE. In these experiments, error limits are assigned based on uncertainties associated with the appearance of the predissociation threshold, the finite rotational temperature of the molecules ($<20~\text{cm}^{-1}$), the linewidth of the OPO laser employed ($\approx10~\text{cm}^{-1}$), and the calibration uncertainty in each spectrum ($<5~\text{cm}^{-1}$). For CeC, PrC, and NdC, the sharp drop to baseline allowed an error limit of $\pm25~\text{cm}^{-1}$ to be assigned to the BDEs. For the BDE of LuC, a slightly larger $\pm30~\text{cm}^{-1}$ error limit was required to account for the broader appearance of the predissociation threshold. A more detailed explanation of the reasoning behind our assignment of error limits has been given previously.^{61,82}

During the experiment measuring the predissociation threshold of LuC, the two-photon ionization

threshold was also measured. In Figure 4, at photon energies near and above 28,395 cm⁻¹, LuC⁺ ion signal began to be observable; at lower energies, however, no LuC ions could be detected. This energy marks the threshold for two-photon ionization of the LuC molecule. Accordingly, doubling the threshold energy (and its assigned error limit) and adding a correction for the shift of the ionization energy due to the electric field in the source region of the TOFMS, which has been measured to be 52 ± 20 cm⁻¹, 62 allows the IE of LuC to be determined as IE(LuC) = 7.05(3) eV. We have recently employed the same methods to measure the ionization energies of RuB, RhB, OsB, IrB, and PtB. 62

Figure 5 displays the predissociation threshold recorded for TmC₂ and its corresponding BDE. For TmC₂, two different ionization schemes were employed to obtain a more precise measurement. The top blue trace displays the TmC_2^+ ion signal recorded with a two-color, two-photon ionization scheme, which is what is typically used for R2PI spectroscopy in our group. For this scan, the molecule was first excited with the tunable output of an OPO excitation laser. After a short delay (~50 ns), the molecule is again irradiated with the output of an exciplex laser operating on KrF (248 nm/5.00 eV). The KrF laser is attenuated so two-photon ionization processes involving just this laser give negligible ion signal. In Figure 5, this signal is labeled " TmC_2^+ OPO + KrF Signal." In this ionization scheme, the two photons used to ionize the molecule are generated by two different lasers interfaced to a timing controller, allowing the delay between the two laser pulses to be precisely controlled. Because the OPO excitation laser was operating at energies that were more than half the ionization energy, the TmC₂ molecules could also be ionized by the absorption of two OPO photons from the same OPO pulse. Ions generated by this one-color R2PI process were formed ~50 ns earlier than the ions generated by the two-color scheme, giving peaks in the time-of-flight mass spectrum that were shifted lower in apparent mass. As a result, the TmC_2^+ mass spectral peak was doubled, with the peak at the lower apparent mass due to the OPO + OPO R2PI process, while the peak at higher apparent mass was due to the OPO + KrF two-color R2PI process. These two signals were easily distinguished because Tm is monoisotopic, so no overlap with other isotopes could occur. The one-color OPO + OPO mass peak was also monitored, giving the signal displayed as the black, middle trace in Figure 5 labeled "TmC₂+ OPO only signal."

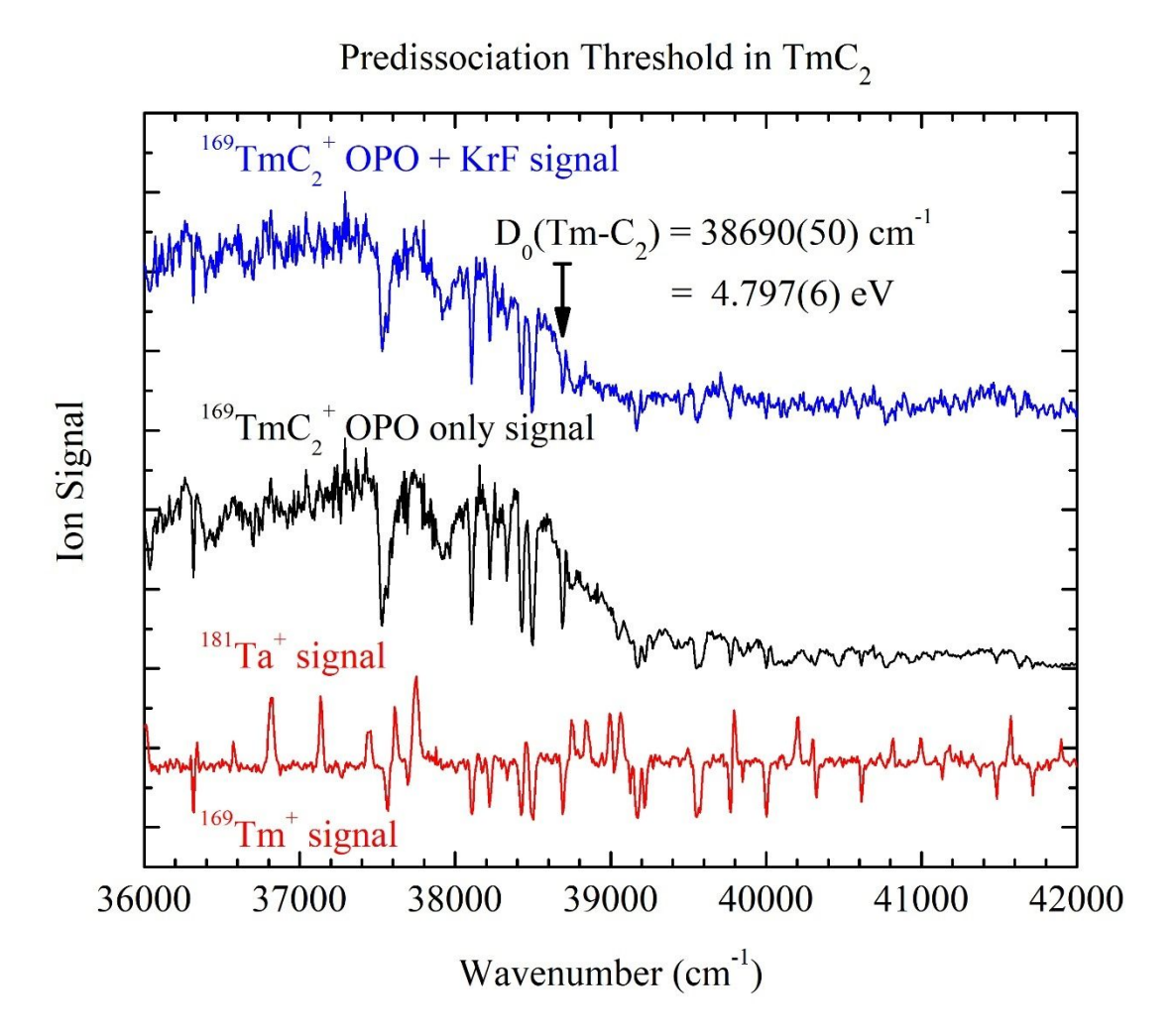


Figure 5. R2PI spectrum of TmC_2 with its predissociation threshold at 38 690(50) cm⁻¹. The top, blue trace provides the predissociation threshold of TmC_2 collected with a time-delayed (~50 ns) two-color two-photon ionization scheme. The middle, black trace displays TmC_2 ion signal in the same energetic vicinity as the top trace, but with a one-color two-photon ionization scheme in which both photons were absorbed from the same ~5 ns duration laser pulse. The atomic spectra of Ta and Tm (bottom trace) were used for calibration (see text for details).

The OPO-only trace (shown in black in Figure 5) requires that the molecule can be excited and ionized within the same \sim 5 ns OPO laser pulse. As a result, excited states that survive for a few ns can be detected in this trace. In contrast, the OPO + KrF ion signal requires that states excited by the OPO laser must survive for 50 ns to be ionized by the delayed KrF laser pulse. For this reason, the OPO-only ion signal displays a drop to baseline near 39,020 cm⁻¹, while the OPO + KrF ion signal decays to baseline near 38,690 cm⁻¹. In the intervening range (38,690 – 39,020 cm⁻¹) some excited states survive long enough to be ionized during the \sim 5 ns OPO laser pulse, but decay before the KrF laser can be fired approximately 50 ns later. For this reason, we assign the TmC₂ predissociation threshold and Tm-C₂ BDE according to the data from the delayed ionization trace, giving D₀(Tm-C₂) = 38,690 ± 50 cm⁻¹ or 4.797(6) eV. We have similarly found a delayed ionization scheme to be necessary in previous studies of the BDEs of the triatomic transition metal diborides, MB₂.⁷²

The lowest trace in Figure 5, in red, deserves comment. Our thulium sample had a small amount of tantalum as an impurity, probably because the molten Tm metal had at one time been in contact with a tantalum crucible or mold. By monitoring the tantalum atomic transitions during the scan, a convenient calibration signal was recorded for use in calibrating the wavenumber axis. While doing so, however, intense atomic transitions in ¹⁶⁹Tm generated a ringing signal that caused the signal at the mass of ¹⁸¹Ta to become negative. The result is the trace recorded for ¹⁸¹Ta also displays ¹⁶⁹Tm atomic transitions as downward-going peaks, allowing both atomic spectra to be used for calibration purposes. These atomic Tm transitions were so intense that they also affected the TmC₂ signal, leading to sharp down-going spikes that are particularly obvious in the 38,000-38,800 cm⁻¹ range.

It is worth noting that the TmC_2 dissociation process observed could be either loss of atomic carbon, forming TmC + C, or loss of C_2 , forming $Tm + C_2$. These two processes are related by the thermochemical cycle

$$D_0(TmC-C) + D_0(TmC) = D_0(Tm-C_2) + D_0(C_2),$$
(3.1)

which may be rewritten as

$$D_0(Tm-C_2) - D_0(TmC-C) = D_0(TmC) - D_0(C_2).$$
(3.2)

The BDE of C_2 is well-established to be 6.24 eV⁸³ and using a B3LYP/Stuttgart ANO computational methodology (Section III), we calculate the BDE of diatomic TmC to be 1.91 eV. We can be confident that the right hand side of (3.2) is negative, so that the lowest dissociation pathway for Tm C_2 is loss of an intact C_2 molecule. This is why we assign the measured Tm C_2 predissociation threshold as D_0 (Tm- C_2).

IV. DISCUSSION

A. Derived Quantities and Comparison to Previous Work

By employing the thermochemical cycle demonstrated in Eqn. 1.1, the cationic BDE of LuC⁺ and the ionization energies of PrC and NdC can be derived using data from the literature. Unfortunately, the BDEs of CeC⁺ and TmC₂⁺ are not available in the literature; neither are the adiabatic IEs of CeC and TmC₂ currently known. In the case of LuC, combining our measurements of D₀(LuC) = 3.685(4) eV and IE(LuC) = 7.05(3) eV with the known IE(Lu) = 5.425871(12) eV⁴² into Eqn. 1.1, we obtain D₀(Lu⁺-C) = 2.06(3) eV. In related work, Guided Ion Beam Mass Spectrometry (GIBMS) has been used by Ghiassee *et al.* to measure the BDEs of PrC⁺ and NdC⁺.^{84,85} These studies report BDEs of D₀(Pr⁺-C) = 2.97(10) eV and D₀(Nd⁺-C) = 2.61(30) eV. Again using Eqn 1.1, these cationic BDEs may be combined with our measured neutral BDEs and the atomic ionization energies of IE(Pr) = 5.4702(4) eV and IE(Nd) = 5.5250(6) eV⁴² to give IE(PrC) = 6.55(10) eV and IE(NdC) = 6.51(30) eV. These results are summarized in Table 1.

Table 1. Experimental and Derived Thermochemical Values for PrC, NdC, and LuC

Molecule	$D_0(LnC)\ (eV)^a$	$D_0(Ln^+-C)$ (eV)	IE(Ln)e	IE(LnC)
CeC	4.893(3)	unknown	5.5386	unknown
PrC	4.052(3)	2.97(10) ^b	5.4702	6.55(10) ^d
NdC	3.596(3)	2.61(30) ^c	5.5250	6.51(30) ^d
LuC	3.685(4)	2.06(3) ^d	5.4258	$7.05(3)^a$

^a Bond dissociation energy for the reaction LnC \rightarrow Ln + C, measured in the present study.

Another set of derived quantities that can be readily obtained are the 0K enthalpies of formation of the gaseous carbides and TmC₂. This is done by using the relationships

$$\Delta_{f}H_{0K}^{\circ}(MC, g) = \Delta_{f}H_{0K}^{\circ}(M, g) + \Delta_{f}H_{0K}^{\circ}(C, g) - D_{0}^{\circ}(MC)$$
(4.1)

and
$$\Delta_{f}H_{0K}^{\circ}(TmC_{2}, g) = \Delta_{f}H_{0K}^{\circ}(Tm, g) + \Delta_{f}H_{0K}^{\circ}(C_{2}, g) - D_{0}^{\circ}(Tm-C_{2})$$
 (4.2)

in combination with the tabulated formation enthalpies of the gaseous metal atoms, C(g), and $C_2(g)$. The results are given in Table 2.

Table 2. Derived 0K Enthalpies of Formation for LnX

Chemical	$\Delta_{\rm f}H_{0\rm K}^{\circ}({\rm Ln,g})$	$\Delta_f H_{0K}^{\circ}(X, g)$	D ₀ (Ln-X)	$\Delta_f H_{0K}^{\circ}(LnC, g)$
Species, LnX	(kJ/mol) a	(kJ/mol) ^b	(kJ/mol) ^c	(kJ/mol)
CeC	423.2(4.2)	711.404(0.044)	472.11(0.29)	662.5(4.2)
PrC	356.8(2.1)	711.404(0.044)	390.96(0.29)	677.2(2.1)
NdC	328.5(2.1)	711.404(0.044)	346.97(0.29)	692.9(2.1)
LuC	427.8(1.7)	711.404(0.044)	355.55(0.29)	783.7(1.7)
TmC_2	233.4(4.2)	820.005(0.092)	462.85(0.58)	590.6(4.2)

^a From Reference ⁸⁶.

^b From Reference 84

^c From Reference 85

^d Derived from Eqn. 1.1. Derived quantities are given in **bold**.

e From Reference 42

^b From Reference ⁸⁷.

^c This work.

In previous Knudsen effusion studies, the BDE of CeC has been measured to be 4.68(30) eV,²⁹ 4.53(22) eV,³⁰ and 4.57(12) eV.³¹ Our value is 0.36 to 0.21 eV higher than these previous measurements. Similarly, the value of $D_0(Tm-C_2)$ has been previously reported as 5.43(46) eV.²⁶ Our study revises this value downward by 0.63 eV, a substantial correction. Knudsen effusion measurements are notoriously difficult and prone to error beyond the quoted error limits, due to difficulties in pressure and temperature calibration, the need for assumptions about the populated electronic states of the molecules, and issues related to the metal atom activity in the gas phase. In previous studies of transition metal carbides, we have found differences between our measured values and Knudsen effusion results ranging from +0.37 eV to -1.02 eV.^{32,88-91} These difficulties are further compounded when polyatomic molecules such as TmC_2 are investigated.

B. Molecular Orbital Structure of LaC, CeC, PrC, NdC, and LuC

The overall molecular orbital (MO) structure of LaC, CeC, PrC, NdC, and LuC is similar to that of the transition metal-p-block diatomic molecules. 32,60,92 However, the lanthanides, of course, also place electrons in the 4f orbitals. A depiction of the LnC MO structure, calculated using B3LYP/cc-pVTZ-DK3, is illustrated in Figure 6 for the example of the $^4\Pi_{5/2}$ ground state of LuC. In Figure 6, the valence MOs of LuC are labeled by the symmetry (σ , π , δ) of each MO and are numbered according to their energy ordering. The lowest energy MO, the 1σ MO, is mainly composed of the 2s orbital on carbon with very minor contributions from the 5d σ and 4f σ orbitals of the lanthanide atom and is nonbonding. The next higher energy MO for LuC is the 2σ MO, which exhibits a bonding interaction between a hybrid $5d\sigma/4f\sigma$ orbital of the lanthanide and the $2p_z$ orbital of the carbon. Next are a degenerate pair of π -bonding orbitals (labeled as 1π) comprising $5d\pi/4f\pi$ hybrid orbitals on the lanthanide and $2p\pi$ orbitals on the carbon atom. The 3σ MO may be considered to be mainly nonbonding, as it is chiefly composed of the 6s and $5d\sigma$ orbitals on the lanthanide atom with a very small contribution of $2p_z$ character from the carbon atom. Likewise, the degenerate 1δ orbitals can be considered to be entirely nonbonding, as they are nearly pure $5d\delta$ orbitals from the lanthanide atom. Moving up in energy are the antibonding MOs (labeled as 2π

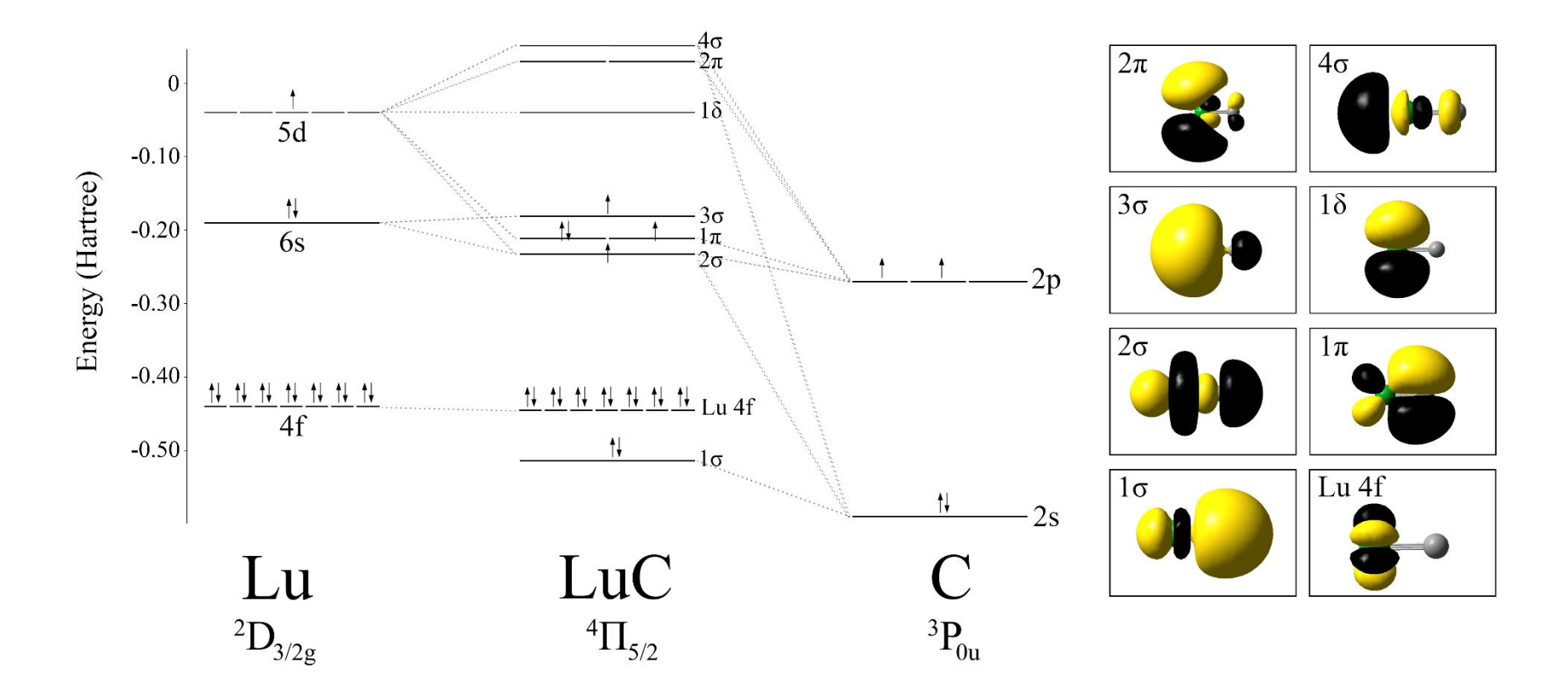


Figure 6. Molecular orbital diagram of LuC in its ${}^4\Pi_{5/2}$ electronic ground state calculated with B3LYP/cc-pVTZ-DK3.

and 4σ) of the LnC species, which are unoccupied in the ground states of LaC, CeC, PrC, NdC, and LuC. The 2π and 4σ antibonding MOs are primarily composed from the same atomic orbitals as the 1π and 2σ bonding MOs, respectively.

C. Chemical Bonding in LaC, CeC, PrC, NdC, and LuC

The electronic ground states and configurations along with various other pertinent properties of LaC, CeC, PrC, NdC, and LuC have been calculated using B3LYP/cc-pVTZ-DK3 (Section II B). For LaC, CeC, PrC, and NdC, it is found that each molecule has the same $1\sigma^2 2\sigma^1 1\pi^4$ ground state electronic configuration but with different occupancies of the 4f-orbitals, giving each molecule a nominal bond order of 2.5. LaC, CeC, PrC, and NdC are calculated to have ground state symmetries and electronic configurations of $^2\Sigma^+$, $1\sigma^2 2\sigma^1 1\pi^4$; $^3\Delta_1$, $1\sigma^2 2\sigma^1 1\pi^4 [\delta^1]$; $^4H_{7/2}$, $1\sigma^2 2\sigma^1 1\pi^4 [\delta^1]$; and 5I_4 , $1\sigma^2 2\sigma^1 1\pi^4 [\pi^1 \delta^1]$, respectively, with the 4f orbital occupancies given in square brackets. For LuC, $^4\Pi_{5/2}$, $1\sigma^2 2\sigma^1 3\sigma^1 1\pi^3$ was calculated for the ground state term and configuration. Because LuC places an electron in the mainly nonbonding Lu-centered 3σ orbital instead of completely filling the 1π bonding MOs as LaC, CeC, PrC, and NdC do, the LuC molecule may be considered to have a bond order of 2. The occupation of the 6s-like 3σ orbital in the ground state of LuC is undoubtedly a result of the much greater relativistic stabilization of this orbital in Lu (\sim 12%), as compared to the early lanthanide atoms La, Ce, Pr, and Nd (\sim 5%). These results, along with our measured and calculated BDEs, calculated bond lengths, and calculated harmonic frequencies are listed in Table 3.

Table 3. Experimentally Measured and Calculated Properties of LaC, CeC, PrC, NdC, and LuC

Molecule	D ₀ (eV)	D ₀ (calc) (eV) ^a	Spin-orbit Correction (eV) ^b	D ₀ (calc) with S-O correction (eV)	r _e (Å) ^c	$\omega_{\rm e}({\rm cm}^{-1})^{\rm c}$	Ground State ^c	Ground Configuration ^c
LaC	4.718(4) ^d	4.71	-0.078	4.63	1.92	770	$2\Sigma^+$	$1\sigma^2 2\sigma^1 1\pi^4$
CeC	4.893(3)e	4.60	+0.071	4.67	1.89	791	$^3\Delta_1$	$1\sigma^2 \ 2\sigma^1 \ 1\pi^4 \ [\delta^1]$
PrC	4.052(3)e	4.06	-0.077	3.98	1.87	797	$^{4}H_{7/2}$	$1\sigma^2 \ 2\sigma^1 \ 1\pi^4 \ [\delta^1 \ \phi^1]$
NdC	3.596(3)e	3.90	-0.032	3.87	1.86	794	$^5\mathrm{I}_4$	$1\sigma^2 \ 2\sigma^1 \ 1\pi^4 \ [\pi^1 \ \delta^1 \ \phi^1]$
LuC	3.685(4)e	3.48	-0.137	3.34	1.98	720	$^4\Pi_{5/2}$	$1\sigma^2 \ 2\sigma^1 \ 3\sigma^1 \ 1\pi^3 \ [\sigma^2 \ \pi^4 \ \delta^4 \ \phi^4]$

^a Calculated with CCSD(T)/cc-pVTZ-DK3 without a semiempirical spin-orbit correction.

Table 4 provides the orbital compositions of the 2σ and 1π bonding MOs calculated from a full natural bond orbital analysis with B3LYP/cc-pVTZ-DK3. 94, 95 The early LnC molecules, LaC, CeC, PrC, and NdC, display a high level of covalent character in these orbitals with metallic character in the range of 35-45%. This is similar to that found for diatomic UC, where the 2σ orbital is 50.3% U, 49.7% C in character and the 1π orbital is 40.1% U, 59.9% C in character. 96 Similar degrees of f-block metal participation in the bonding orbitals are also found for the pentavalent N=Pr=O molecule and in diatomic UB. 97, 98 For the 1π bonding MO, the $5d\pi_{Ln}$, $4f\pi_{Ln}$, and $2p\pi_{C}$ orbital contributions for La, Ce, Pr, and Nd are quite similar. In contrast, the 2σ bonding MO displays a systematic variation in the lanthanide $5d\sigma$ and $4f\sigma$ orbital contributions. Lanthanum carbide has the greatest $5d\sigma$ and least $4f\sigma$ orbital contribution to the 2σ bonding MO. The amount of $5d\sigma$ character then decreases and

^b See text and Supplementary Information.

 $[^]c$ Calculated with B3LYP/cc-pVTZ-DK3 on the Ln constituents and aug-cc-pVTZ-DK on the carbon atom. In the ground configuration column, the orbitals within the square brackets are the symmetries of the f-orbital occupancies of the ground state. The symbols r_e and ω_e refer to the bond length and harmonic frequency of the LnC molecule.

^d Measured in Reference 32.

^e Measured in the present study.

Table 4. Orbital Composition Analysis of the Bonding MO's in LaC, CeC, PrC, NdC, and LuCa

	2σ Molecular Orbital				1π Molecular Orbital			
		Ln		C	L	n	C	
Molecule	6sσ	5dσ	4fσ	$2s/2p\sigma$	5dπ	4fπ	2pπ	
LaC		34%	6%	51%	33%	2%	65%	
CeC		30%	10%	50%	34%	4%	62%	
PrC		27%	14%	50%	32%	7%	60%	
NdC		23%	21%	49%	38%	6%	55%	
LuC	20%	7%		64%	20%		78%	

^a Calculated with B3LYP/cc-pVTZ-DK3 on the Ln constituents and aug-cc-pVTZ-DK on the carbon atom. Note: The calculated contributions for the 2σ orbital do not add up to 100%. The remaining contributions are entirely on the Ln atom, coming from the Ln 5s, 5pσ, and primarily the 6pσ atomic orbitals. Thus, the 2σ orbital in LaC, CeC, PrC, and NdC is very nearly 50% Ln in character.

the amount of 4f σ character increases as one moves through the series of early lanthanide carbides LaC, CeC, PrC, and NdC, reflecting the increasing stabilization of the 4f orbitals as one traverses the early lanthanide series. The increasing stabilization of the 4f orbitals as one traverses the early lanthanide series, relative to the 5d orbitals, is explained with reference to atomic energy level data in the Supporting Information, and is illustrated in Figure S1. Another way to view this is to recognize that as one moves across the 4f series, the energy required to access the 5d-orbitals increases, with the notable exceptions of Gd, Tb, and Lu. Thus, the adiabatic bond energies of these molecules are expected to decrease as one moves across the series because the 4f orbitals are much more compact than the 5d orbitals, leading to less effective chemical bonding as the 5d character is replaced with 4f character.

Along with the orbital compositions of the MOs in the LnC molecules, we have also calculated the natural charges and natural electron occupancies of the lanthanide constituents of these molecules using the previously mentioned full natural bond orbital analysis, ^{94, 95} which are given in Table 5. The computed natural charges demonstrate that the lanthanide atoms in LaC, CeC, PrC, NdC, and LuC exhibit a +1

oxidation state in bonding with a carbon atom. Therefore, the atomic charge distribution in this family of LnC molecules can generally be described as Ln⁺¹ C⁻¹. Moreover, the natural electron occupancies reveal that La, Ce, Pr, and Nd all have a 6s⁰5d² electronic configuration when bonding with a carbon atom. Lutetium differs, however. It bonds with a carbon atom from its Lu⁺, 6s¹5d¹ electronic configuration due to the greater relativistic stabilization of the 6s orbital in lutetium.⁹³ This is consistent with the fact that the 3σ nonbonding orbital, which is predominantly 6s in character, is singly occupied in LuC while it is completely vacant in LaC, CeC, PrC, and NdC.

Table 5. Natural Charges and Natural Electron Configurations for the Lanthanide Atoms in LaC, CeC, PrC, NdC, and LuC^a

Lanthanide Atom	Natural Charge	Natural Electron Occupancies				
Lanthanide Atom	Natural Charge	6s	4f	5d		
La	+0.98	0.03	0.17	1.94		
Ce	+0.94	0.04	1.22	1.91		
Pr	+0.92	0.04	2.33	1.82		
Nd	+0.92	0.04	3.34	1.80		
Lu	+0.86	0.94	[core]	1.13		

^a The natural charges and natural electron occupancies were calculated using the Natural Atomic Orbital Molecular Orbital (NAOMO) methodology within the Gaussian 16 software package with B3LYP/cc-pVTZ-DK3 on the Ln constituents and aug-cc-pVTZ-DK on the carbon atom.

Table 3 shows that there is a significant variation in the bond strengths of LaC (4.718(4) eV), CeC (4.893(3) eV), PrC (4.052(3) eV), and NdC (3.596(3) eV), even though the molecules have almost identical ground state electronic configurations, differing only in the occupancy of the 4f orbitals.

Moreover, LaC, CeC, PrC, and NdC also have very similar calculated bond lengths and harmonic stretching frequencies, 1.92Å/770 cm⁻¹, 1.89 Å/791 cm⁻¹, 1.87 Å/797 cm⁻¹, and 1.86 Å/794 cm⁻¹, respectively. The slight differences in bond lengths of these molecules are likely due to the lanthanide contraction, ⁹⁹ while the variations in harmonic frequency result from a combination of the lanthanide contraction and the changes in reduced mass. The similar electronic structure of these molecules presents

a conundrum, however: Why is there a roughly 1.30 eV range of BDEs across the succession from LaC to NdC, when the molecules themselves have virtually identical ground state electronic configurations, bond lengths, and fundamental vibrational frequencies?

We propose that this conundrum may be resolved by considering the diabatic limits to which the ground molecular states correlate. We have previously found that by considering the dissociation to the appropriate diabatic separated atom limits, the anomalous trends in bond dissociation energies found in the lanthanide sulfides, lanthanide selenides, and the late transition metal borides, MB, can be well-understood. $^{57, 62, 92}$ The fact that these four molecules exhibit natural charges of Ln^+C^- implies that they diabatically dissociate to a $Ln^+ + C^-$ separated ion limit. Further, the natural electron configurations of $5d^2 4f^6 6s^6$ correspond to excited states of the Ln^+ ion. Thus, the diabatic dissociation limits for LaC, CeC, PrC, and NdC must correspond to configurations of the Ln^+ ion of $La^+ 5d^2$, $Ce^+ 5d^24f^3$, $Pr^+ 5d^24f^2$, and $Nd^+ 5d^24f^3$. The lowest known energy levels corresponding to these configurations are $La^+ 5d^2$, $^5F_{2g}$ at 0.00 cm^{-1} ; $Ce^+ 5d^2 4f^3$, $^4H_{7/2u}$ at 0.00 cm^{-1} ; $Pr^+ 5d^2 4f^2$, $^5L_{6g}$ at 5854.61 cm^{-1} ; and $Nd^+ 5d^2 4f^3$, $^6M_{13/2u}$ at 8009.81 cm^{-1} . It may readily be verified that when these terms combine with the ground $^4S_{3/2u}$ level of the C^- ion, the ground states of LaC ($^2\Sigma^+$), CeC ($^3\Delta_1$), PrC ($^4H_{7/2}$), and NdC (5I_4) are among the states generated. The bond dissociation energy measured to this diabatic limit, which we have termed the intrinsic bond dissociation energy (IBDE), is then given by:

$$IBDE(LnC) = D_0(LnC) + IE(Ln) + PE(Ln^{+1}) - IE(C).$$
 (4.3)

The calculated values of intrinsic bond dissociation energy (IBDE) are provided in Table 6.

Table 6. Intrinsic Bond Dissociation Energies (IBDE) of LaC, CeC, PrC, NdC, and LuC.

Molecule (LnC)	$D_0(LnC)$ (eV)	Ln IE (eV) ^a	EA(C) (eV) ^b	Ln PE (eV) ^a	IBDE (eV) ^c
LaC	4.718(3) ^d	5.5769	1.2621	$0.000^{\rm e}$	9.033 (3)
CeC	$4.893(3)^{f}$	5.5386	1.2621	$0.000^{\rm e}$	9.170(3)
PrC	4.052(3) ^b	5.4702	1.2621	0.726	8.986(3)
NdC	3.596(3)b	5.5250	1.2621	0.993	8.852(3)
LuC	3.685(4) ^b	5.4258	1.2621	1.463	9.311(4)

^a From Reference 42. IE(Ln) refers to the ionization energy of the Ln atom; PE refers to the energy required to excite the Ln⁺ ion to the appropriate diabatic limit for bonding.

In the case of LuC, the natural bond orbital analysis results show that the diabatic dissociation limit for this species is Lu⁺, 5d¹ 6s¹, for which the lowest energy level is ${}^{3}D_{1}$ at 11796.24 cm⁻¹. 42 Again, the calculated LuC ground state, ${}^{4}\Pi_{5/2}$ is generated when this level combines with the C⁻⁴S_{3/2u} ground level. Hence, its IBDE has also been calculated using Eq. 4.3, and is likewise listed in Table 6.

When measured to the appropriate diabatic limit, the conundrum of the wide variation in BDEs of the electronically similar molecules LaC, CeC, PrC, and NdC is solved. Rather than a range of BDEs spanning 1.3 eV, now the range in IBDEs is reduced to 0.32 eV. Further, there is now a nearly smooth trend of slightly decreasing IBDE as one traverses the early lanthanide carbides. This is consistent with the reduced 5d character in the 2σ bonding orbital as one moves across this series of closely related molecules (see Table 4). The BDEs and IBDEs of these species are plotted in Figure 7 for a direct visual comparison.

^b From Reference 43. EA(C) refers to the electron affinity of the carbon atom.

^c IBDE is defined in Eqn. 4.3

^d From Reference 32.

^e La⁺ and Ce⁺ both have a d² configuration in their ground states, so no promotion is required to prepare these ions for bonding.

^f From this work.

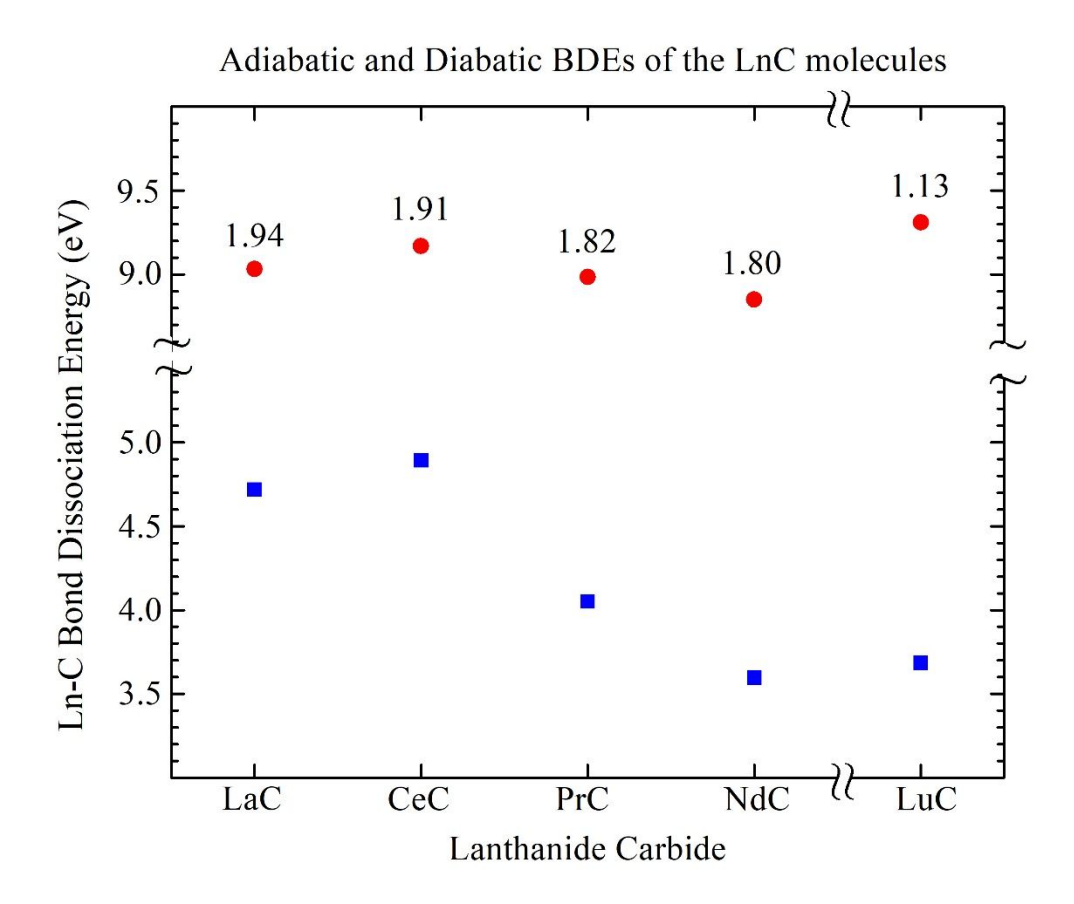


Figure 7. Bond dissociation energies of the LnC (Ln = La, Ce, Pr, Nd, Lu) molecules. The BDE for LaC is from Ref. 32. The square blue symbols on the bottom provide the adiabatic BDEs of the LnC molecules and the red circles in the upper trace provide the corresponding diabatic BDEs. Both are plotted on the same scale, but note the break in the y-axis between 5.5 and 8.5 eV. The diabatic BDEs are obtained from equation 4.3 (see text). The natural orbital occupancies of the 5d orbitals in the various LnC molecules are given above the red circles that provide the diabatic BDEs, ranging from 1.94 electrons in LaC to 1.13 electrons in LuC.

It is interesting that the BDE of LuC is among the smaller values for this set of molecules, but the diabatic BDE (IBDE) is the largest of the set. This is true despite the fact that this species has a nominal bond order of 2 while the others have a nominal bond order of 2.5. LuC also has the largest calculated bond length and lowest calculated harmonic frequency of the set. In addition, owing to the high stability of the $6s^2$, ${}^{1}S_{g}$ ground state of the Lu⁺ ion, it has the least amount of 5d character in its 2σ and 1π bonding orbitals of the set. It is well known that bond order is imperfectly correlated with the strength of the bond, and, as has been observed most dramatically in studies of the Cp₂UO vs. Cp₂UNMe molecules. 100 In the case of LuC, this anomalous behavior likely results from the placement of a single electron in the 6s-like 3σ orbital, which is much more polarizable than the 5d or 4f orbitals. The greater polarizability of this orbital may allow the incoming C^- anion to feel more of the underlying charge of the Lu⁺ cation. A more detailed analysis of the chemical bonding would be required to confirm this conjecture.

D. Electronic Structure and Chemical Bonding of TmC₂

Figure 8 shows the MO diagram of the TmC_2 molecule in its 2B_1 ground electronic state. The molecule is best considered by combining an isolated Tm atom with an intact C_2 unit, as these are the fragments produced at the lowest dissociation limit. This is the viewpoint adopted in Figure 8, where the MOs of the C_2 molecule in its ${}^1\Sigma_g^+$ ground electronic state are listed on the right side of the figure. The 4f orbitals of Tm are scattered throughout the energy range of the other MOs of TmC_2 . With one exception, discussed below, the 4f orbitals of Tm make only tiny contributions to the natural bond orbitals of the molecule. The atomic compositions of the MOs displayed in Figure 8 are provided in Table 7.

The $1a_1$ MO is a mostly nonbonding and energetically buried MO, with minimal interaction between the Tm atom and the $1\sigma_g$ bonding, 2s-based MO orbital of the C_2 ligand. This is because the $1\sigma_g$ MO of C_2 is energetically too widely separated from the Tm AOs for significant interaction. Skipping over the 4f orbitals, the next orbital in order of increasing energy is the $1b_2$ MO, which exhibits an inphase weakly bonding interaction between the d_{yz} AO on Tm and the $1\sigma_u$ antibonding MO of the C_2 molecule. Given that the Tm 5d and 4f atomic orbitals only contribute a total of 6% character to this

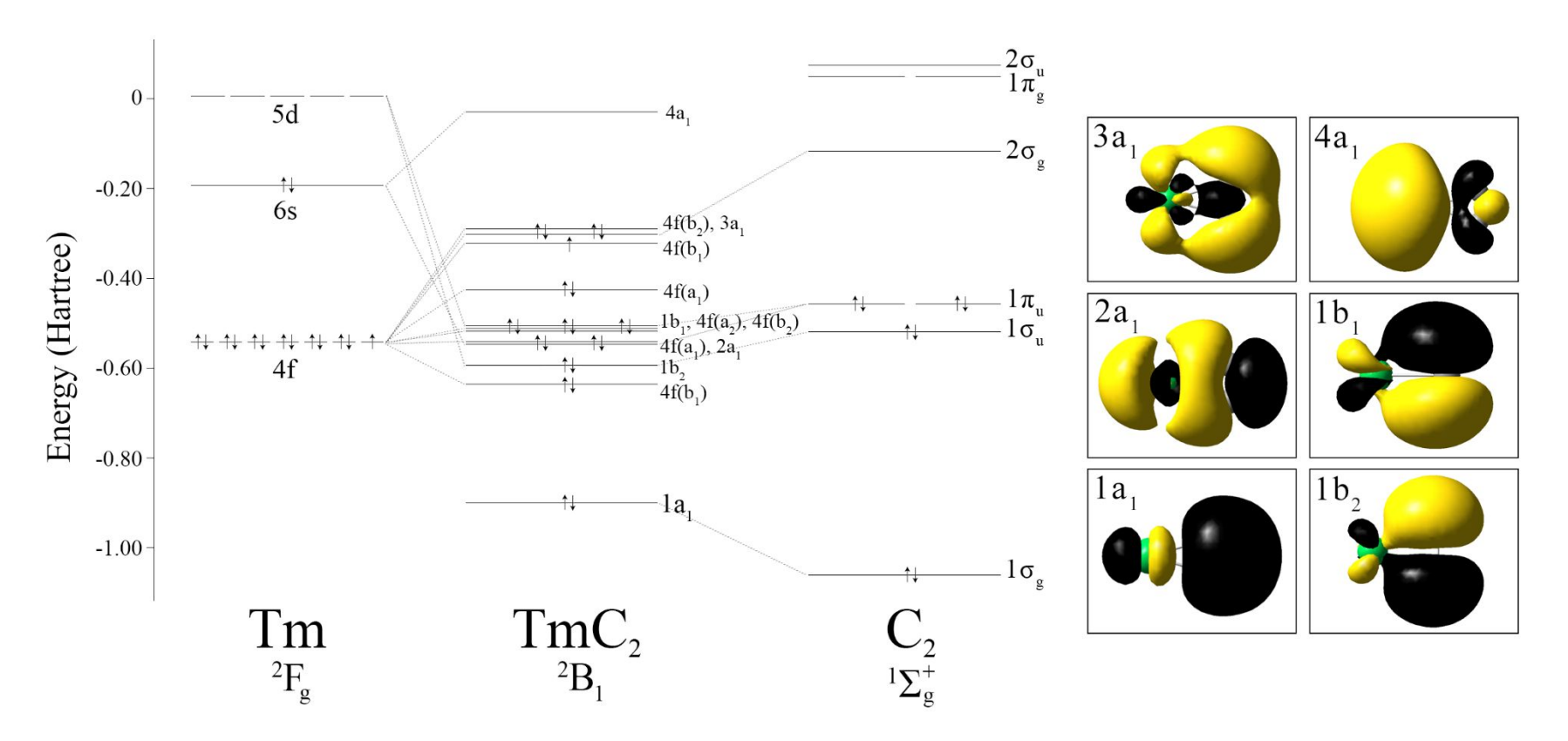


Figure 8. Left: Quantitative molecular orbital diagram of TmC_2 and its 2B_1 electronic ground state calculated with B3LYP/Stuttgart RSC ANO. Right: Image depictions for the relevant MOs of TmC_2 . For all of the images of the MOs, except the $1b_1$ MO image, the z-axis runs along the molecular axis, *i.e.* from left to right, the y-axis runs up and down, and the x-axis projects out of the plane. In the $1b_1$ MO image, the TmC_2 molecule is rotated 90° about the molecular z-axis so that the C_2 ligand (y-axis) projects out of the plane of the figure.

Table 7. Orbital Composition Analysis of the Orbitals of TmC₂ ^a

		Tm			C_2	
Orbital	6s	5d	4f	6p _z	2s	2p
1a ₁		1%			68%	26%
$1b_2$		3%	3%		50%	40%
$2a_1$	10%	3%	5%			78%
$1b_1$		4%	2%			92%
$3a_1$	7%	1%	36%		13%	41%
$4a_1$	63%	1%		16%		14%

^a Calculated with B3LYP/Stuttgart RSC ANO. The calculated natural atomic charge on Tm is +1.3130, and each C atom has a natural charge of -0.6565. The natural electronic configuration is 6s^{0.43} 4f^{12.96} 5d^{0.27}.

orbital, it is probably best characterized as nonbonding or at most very weakly bonding. The $2a_1$ MO can be characterized mostly as an in-phase interaction of the 6s AO on Tm with the $1\pi_u$ bonding MO on the C_2 molecule. As 18% of the character of this orbital originates in Tm atomic orbitals, it is fair to call this a bonding MO. The $1b_1$ MO similarly involves an in-phase interaction between the second $1\pi_u$ bonding orbital of C_2 and the d_{xz} AO on Tm. As this orbital also has only 6% Tm character, it is primarily nonbonding, or at most very weakly bonding in character, like the $1b_2$ orbital. The $1b_2$, $2a_1$, and $1b_1$ MOs are all examples of the C_2 ligand weakly donating electron density into AOs on the Tm atom. In contrast, in the $3a_1$ MO the Tm atom donates electron density into the completely vacant $2\sigma_g$ bonding MO on the C_2 ligand. More interesting is the fact that the thulium atomic contribution (net 44%) to the $3a_1$ MO is dominated by 4f character (36%). Finally, although the $4a_1$ MO is unoccupied in the ground state of TmC, it is included in Figure 8 and Table 7 to demonstrate that it is almost entirely Tm 6s and $6p_z$ in character with little contribution from the C_2 molecule.

The lack of electrons in the $4a_1$ orbital, which is primarily a polarized 6s Tm orbital, suggests that the Tm atom may be divalent in this molecule, leading to an assignment of the species as a $Tm^{2+}C_2^{2-}$ ionic species, consistent with the ground state of the Tm^{2+} ion of $4f^{13}$ $6s^0$, ${}^2F_{7/2u}$. 42 The natural orbital bond analysis, however, gives natural atomic charges of $Tm^{+1.313}$ and $C_2^{-1.313}$, indicating a structure intermediate between Tm^+ and Tm^{2+} . Table 8 provides experimentally measured and calculated properties for TmC_2 as well as computed bond lengths and fundamental stretching frequencies for the isolated C_2 and C_2^{-2}

Table 8. Experimentally Measured and Calculated Properties of TmC₂

		D ₀ (calc.)	Ground State and	$r_e (\text{Å})^c$		$v (cm^{-1})^c$		
Molecule	$D_0 (eV)^a$	$(eV)^b$	Configuration ^c	Tm-	C-C	CTmC Bend	Tm-C ₂ Stretch	C-C Stretch
			25 /4 2 44 2 44 2			Dena	Suetch	Suetch
TmC_2	4.797(6)	4.46	${}^{2}B_{1}/1a_{1}{}^{2} 1b_{2}{}^{2} 1b_{1}{}^{2}$ $2a_{1}{}^{2} 3a_{1}{}^{2} [a_{1}{}^{4} a_{2}{}^{2}]$	2.26	1.26	373	452	1809
			$b_1^3 b_2^4$					
C_2			$^{1}\Sigma_{g}^{+}/1\sigma_{g}^{2}1\sigma_{u}^{2}1\pi_{u}^{4}$		1.24			1874
C ₂ -2			$\frac{{}^{1}\Sigma_{\mathrm{g}}^{+}/{1}\sigma_{\mathrm{g}}^{-2}}{2\sigma_{\mathrm{g}}^{-2}}\frac{{1}\sigma_{\mathrm{u}}^{-2}}{1\pi_{\mathrm{u}}^{4}}$		1.27			1769

^a D_0 is the bond dissociation energy for $TmC_2 \rightarrow Tm + C_2$, measured in the present study.

molecules. The C-C bond length (1.26 Å) in the TmC_2 molecule demonstrates that the carbon bond in the TmC_2 molecule is somewhere between a double bond and a triple bond.¹⁰¹ The C-C bond length and vibrational frequency calculated in TmC_2 are intermediate between those calculated for the isolated C_2 and C_2^{2-} species, consistent with the NBO charge on the C_2 moiety of -1.313.

The chemical bonding and thermochemical stability of MC_2/LnC_2 species have long been compared to the bonding and thermochemical stability of MO/LnO species because there are four 2p electrons available in each ligand for bonding to a metal atom in these species. The idea of "pseudo oxygen" character for the C_2 ligand when bonding with metal atoms is noted by the correlation of the -O and $-C_2$ electron affinities and the dipole moments and bond dissociation energies of the corresponding MO and MC_2 species. $^{39,\ 102-105}$ The BDE of TmO has been measured previously by our group to be $5.242(6)~eV^{61}$ and the BDE of Tm C_2 is reported in this current work as 4.797(6)~eV. It has been suggested that the TmO ground state correlates to the $Tm^+\ 4f^{12}\ 5d^1\ 6s^1 + O^-\ 2p^5,\ ^2P_u$ separated ion limit. 57 If this is correct, the 0.445(8)~eV difference between the bond strengths of TmO and TmC_2 may result

^b Calculated with CCSD(T) with the Stuttgart RSC ANO basis set on the Ln atom and aug-cc-pVQZ atom on the carbon atoms.

 $^{^{\}rm c}$ The equilibrium bond lengths, $r_{\rm e}$, and harmonic vibrational frequencies, v, were calculated using the B3LYP density functional and the Stuttgart RSC ANO basis set on the Ln atom and the aug-cc-pVQZ basis set on the carbon atoms. In the ground configuration column, the orbitals within the square brackets are the 4f orbital occupancies of the TmC_2 molecule.

from the greater amount of 5d character in the bonding MOs of TmO compared to the MOs of TmC₂, allowing a stronger bond to be formed.

Table 8 shows that the Tm- C_2 BDE calculated using the CCSD(T) method with the Stuttgart RSC ANO basis set on Tm and the aug-cc-pVQZ basis set on C is 4.46 eV, which is substantially less than the measured value of 4.797(6) eV. The agreement between theory and experiment is actually much worse than this comparison indicates, however, because the calculation omits corrections due to spin-orbit interaction. The ground level of the Tm atom is stabilized by -0.466 eV in first-order perturbation theory (see supporting information), while little spin-orbit stabilization is expected in the C_{2v} Tm C_2 molecule. When corrected for the spin-orbit stabilization of the separated atom limit, the computed BDE of Tm- C_2 would be 4.46 eV – 0.466 eV = 3.99 eV, which is 0.8 eV less than the measured value. The magnitude of this error emphasizes the need for further improvements in quantum chemical methodology in order to obtain accurate thermochemistry for lanthanide molecules, particularly when spin-orbit interaction plays an important role.

V. CONCLUSION

The bond dissociation energies of CeC, PrC, NdC, LuC, and TmC₂ have been assigned by the precise measurement of their respective predissociation thresholds. The identification of the observed predissociation threshold with the thermochemical bond dissociation energy is based on the principle that the density of excited electronic states at the ground separated atom limit is so high that spin-orbit and nonadiabatic interactions allow the molecule to hop from one potential energy surface to another quite effectively, rapidly finding a path to ground state fragments as soon as the bond dissociation energy is exceeded. In addition, during the experiments designed to measure the BDE of LuC, the two-photon ionization threshold for LuC was observed, allowing the adiabatic ionization energy of LuC to be measured as well.

From the resonant two-photon ionization spectroscopy experiments and the quantum chemical calculations performed in this work, new fundamental insights on the chemical bond between lanthanides

and carbon have been obtained. The BDEs of LaC (4.718(4) eV), CeC (4.893(3) eV), PrC (4.052(3) eV), and NdC (3.596(3) eV) are all markedly different despite these molecules all having monovalent lanthanide constituents, similar bond lengths and fundamental frequencies, and identical electronic occupancies within their bonding, nonbonding, and antibonding MOs. The wide range of adiabatic BDEs of these molecules derives from the fact that the molecular ground states diabatically correlate to separated ion states of Ln⁺ 4f^h 5d²6s⁰ + C⁻ 2p³, but the promotion energy required to reach this separated ion limit varies across the series of molecules. The BDE measured to the appropriate diabatic separated ion limit shows a greatly reduced range, with the deviations being well-correlated with the amount of 4f vs. 5d character in the bonding σ orbital. The relativistic stabilization of the 6s orbital in Lu causes LuC to have a different ground electronic configuration that the LaC, CeC, PrC, and NdC molecules. In LuC, the 1π bonding orbital lacks one electron of being filled while the mostly nonbonding 3σ orbital is singly occupied.

Thulium dicarbide, TmC₂, is the first lanthanide dicarbide species we have studied using R2PI spectroscopy. A two-color ionization scheme was employed to accurately measure a sharp predissociation threshold for this molecule. The bond dissociation energy of Tm-C₂, 4.797(6) eV, is relatively weak compared to the BDEs of other LnC₂ molecules,^{39, 106} likely due to the high promotion energy (1.63 eV⁴²) required to access an electronic configuration in which Tm has a 5d electron that can more favorably bond with the C₂ ligand. As a result, a considerable amount of 4f character is involved in the 3a₁ bonding HOMO of TmC₂, weakening the bond between Tm and C₂ as compared to the lanthanides that can more readily access the 5d orbitals. It is our hope that these quantitative bond energy measurements and periodic trends can contribute to a deeper understanding of lanthanide inorganic chemistry and to the development of improved computational methods for quantum chemical studies of the 4f elements.

ASSOCIATED CONTENT

Supporting Information

The supporting information is available free of charge at https://pubs.acs.org/doi/...

Excel file providing the spectra displayed in Figures 1-5.

PDF file describing the methods used to approximate spin-orbit corrections to the calculated BDEs, also presenting an analysis of the relative stabilization of the 4f orbitals over the 5d orbitals as the lanthanide series is traversed and a table providing the HOMO-LUMO gaps for the molecules investigated here.

AUTHOR INFORMATION

Corresponding Author

Michael D. Morse – Department of Chemistry, University of Utah, Salt Lake City, Utah 84112-0850, United States; orcid.org/0000-0002-2386-7315; Email: morse@chem.utah.edu

Authors

Dakota M. Merriles – Department of Chemistry, University of Utah, Salt Lake City, Utah 84112-

0850, United States; orcid.org/0000-0003-1363-1306; Email: dakota.merriles@chem.utah.edu

Anthony London – Department of Chemistry, University of Utah, Salt Lake City, Utah 841120850, United States; Email: u1088991@utah.edu

Erick Tieu– Department of Chemistry, University of Utah, Salt Lake City, Utah 84112-

0850, United States; orcid.org/0000-0001-9730-3136; Email: erick.q.tieu@gmail.com

Christopher Nielson – Department of Chemistry, University of Utah, Salt Lake City, Utah

84112-0850, United States; orcid.org/0000-0001-7260-3423; Email: cnielson3@gmail.com

Notes

The authors declare no competing financial interest.

ACKNOWLEDGEMENTS

The authors thank the National Science Foundation for support of this research under Grant No.

CHE-1952924. The authors also thank the Center for High Performance Computing at the University of 35

Utah for their technical resources and support.

REFERENCES

- (1) Cotton, F. A. A millennial overview of transition metal chemistry. *Journal of the Chemical Society, Dalton Transactions* **2000**, (13), 1961-1968, 10.1039/B001668N. DOI: 10.1039/B001668N.
- (2) Thayer, J. S. Organometallic Chemistry: A Historical Perspective. In *Advances in Organometallic Chemistry*, Stone, F. G. A., West, R. Eds.; Vol. 13; Academic Press, 1975; pp 1-45.
- (3) Pimentel, G. C.; Spratley, R. D. *Understanding Chemistry*; Holden-Day, 1971.
- (4) Cotton, S. A. Aspects of the lanthanide-carbon σ-bond. *Coord. Chem. Rev.* **1997**, *160*, 93-127. DOI: https://doi.org/10.1016/S0010-8545(96)01340-9.
- (5) Cloke, F. G. N. Zero oxidation state compounds of scandium, yttrium, and the lanthanides. *Chem. Soc. Rev.* **1993**, *22* (1), 17-24, 10.1039/CS9932200017. DOI: 10.1039/CS9932200017.
- (6) Zimmermann, M.; Anwander, R. Homoleptic Rare-Earth Metal Complexes Containing Ln–C σ-Bonds. *Chem. Rev.* **2010**, *110* (10), 6194-6259. DOI: 10.1021/cr1001194.
- (7) Evans, W. J. Organometallic Lanthanide Chemistry. In *Advances in Organometallic Chemistry*, Stone, F. G. A., West, R. Eds.; Vol. 24; Academic Press, 1985; pp 131-177.
- (8) Ortu, F. Rare Earth Starting Materials and Methodologies for Synthetic Chemistry. *Chem. Rev.* **2022**, *122* (6), 6040-6116. DOI: 10.1021/acs.chemrev.1c00842.
- (9) Zhu, Q.; Zhu, J.; Zhu, C. Recent progress in the chemistry of lanthanide-ligand multiple bonds. *Tetrahedron Letters* **2018**, *59* (6), 514-520. DOI: https://doi.org/10.1016/j.tetlet.2017.12.079.
- (10) Bochkarev, M. N. Synthesis, Arrangement, and Reactivity of Arene–Lanthanide Compounds. *Chem. Rev.* **2002**, *102* (6), 2089-2118. DOI: 10.1021/cr010329i.
- (11) Izod, K. Alkyl, carbonyl and cyanide complexes of the group 3 metals and lanthanides. In *Reference Module in Chemistry, Molecular Sciences and Chemical Engineering*, Elsevier, 2021.
- (12) Lyubov, D. M.; Trifonov, A. A. Ln(II) alkyl complexes: from elusive exotics to catalytic applications. *Inorganic Chemistry Frontiers* **2021**, *8* (12), 2965-2986, 10.1039/D1QI00206F. DOI: 10.1039/D1QI00206F.
- (13) Wang, X.; Cho, H.-G.; Andrews, L.; Chen, M.; Dixon, D. A.; Hu, H.-S.; Li, J. Matrix Infrared Spectroscopic and Computational Investigations of the Lanthanide-Methylene Complexes CH₂LnF₂ with Single Ln-C Bonds. *J. Phys. Chem. A* **2011**, *115* (10), 1913-1921. DOI: 10.1021/jp111592e From American Chemical Society . All Rights Reserved. CAPLUS.
- (14) Cantat, T.; Mézailles, N.; Auffrant, A.; Le Floch, P. Bis-phosphorus stabilised carbene complexes. *Dalton Transactions* **2008**, (15), 1957-1972, 10.1039/B717600G. DOI: 10.1039/B717600G.

- (15) Xu, W.; Jin, X.; Chen, M.; Pyykkö, P.; Zhou, M.; Li, J. Rare-earth monocarbonyls MCO: comprehensive infrared observations and a transparent theoretical interpretation for M = Sc; Y; La-Lu. Chem. Sci. **2012**, 3 (5), 1548-1554. DOI: 10.1039/c2sc00998f From American Chemical Society . All Rights Reserved. CAPLUS.
- (16) Gong, Y.; Wang, X.; Andrews, L.; Chen, M.; Dixon, D. A. Infrared Spectra and Quantum Chemical Calculations of the Bridge-Bonded $HC(F)LnF_2$ (Ln = La-Lu) Complexes. *Organometallics* **2011**, *30* (16), 4443-4452. DOI: 10.1021/om200533q From American Chemical Society . All Rights Reserved. CAPLUS.
- (17) Schilling, J. B.; Beauchamp, J. L. Hydrocarbon activation by gas-phase lanthanide cations: interaction of praseodymium (Pr⁺), europium (Eu⁺), and gadolinium (Gd⁺) with small alkanes, cycloalkanes, and alkenes. *J. Am. Chem. Soc.* **1988**, *110* (1), 15-24.
- (18) Cornehl, H. H.; Heinemann, C.; Schroeder, D.; Schwarz, H. Gas-Phase Reactivity of Lanthanide Cations with Hydrocarbons. *Organometallics* **1995**, *14* (2), 992-999.
- (19) Cornehl, H. H.; Hornung, G.; Schwarz, H. Gas-phase reactivity of lanthanide cations with fluorocarbons: C-F versus C-H and C-C-bond activation. *J. Am. Chem. Soc.* **1996**, *118* (41), 9960-9965.
- (20) Marçalo, J.; Santos, M.; Pires de Matos, A.; Gibson, J. K.; Haire, R. G. Gas-Phase Reactions of Doubly Charged Lanthanide Cations with Alkanes and Alkenes. Trends in Metal(2+) Reactivity. *J. Phys. Chem. A* **2008**, *112* (49), 12647-12656. From American Chemical Society . All Rights Reserved. CAPLUS.
- (21) Jian, J.; Zhang, Q.; Wu, X.; Zhou, M. Isocyanate Formation from Reactions of Early Lanthanide Metal Atoms with NO and CO in Solid Argon. *J. Phys. Chem. A* **2017**, *121* (41), 7861-7868. DOI: 10.1021/acs.jpca.7b08586.
- (22) Gong, Y.; Andrews, L.; Chen, M.; Dixon, D. A. Reactions of Late Lanthanide Metal Atoms and Methanol in Solid Argon: A Matrix Isolation Infrared Spectroscopic and Theoretical Study. *J. Phys. Chem. A* **2011**, *115* (51), 14581-14592. DOI: 10.1021/jp209135a From American Chemical Society . All Rights Reserved. CAPLUS.
- (23) Li, Y.; Gong, Y.; Zhou, X.; Su, J.; Li, J.; Zhou, M. Infrared spectroscopic and theoretical study of the reactions of cerium atoms with methanol in solid argon. *J. Mol. Spectrosc.* **2015**, *310*, 50-56. DOI: https://doi.org/10.1016/j.jms.2014.12.013.
- (24) Roos, B. O.; Pyykkö, P. Bonding Trends in Molecular Compounds of Lanthanides: The Double-Bonded Carbene Cations LnCH₂⁺ (Ln=Sc, Y, La-Lu). *Chem.--Eur. J.* **2010**, *16* (1), 270-275. DOI: 10.1002/chem.200902310 From American Chemical Society . All Rights Reserved. CAPLUS.
- (25) Panetti, G. B.; Sergentu, D.-C.; Gau, M. R.; Carroll, P. J.; Autschbach, J.; Walsh, P. J.; Schelter, E. J. Isolation and characterization of a covalent Ce^{IV}-Aryl complex with an anomalous ¹³C chemical shift. *Nature Communications* **2021**, *12* (1), 1713. DOI: 10.1038/s41467-021-21766-4.
- (26) Chandrasekharaiah, M. S.; Gingerich, K. A. Thermodynamic properties of gaseous species. In *Handbook on the Chemistry and Physics of Rare Earths*, Gschniedner, K. A. J., Eyring, L. Eds.; Vol. 12; Elsevier, 1989; pp 409-431.

- (27) Teghil, R.; D'Alessio, L.; Santagata, A.; Ferro, D.; De Maria, G. Pulsed laser ablation of Nd and Pr carbides. *Applied Surface Science* **2003**, *208-209*, 119-124. DOI: https://doi.org/10.1016/S0169-4332(02)01347-8.
- (28) Pelino, M.; Gingerich, K. A. Atomization energies of the gaseous molecules LaC and La₂C by high temperature equilibrium measurements. *J. Phys. Chem.* **1989**, *93* (4), 1581-1583.
- (29) Gingerich, K. A. Mass-Spectrometric Evidence for the Molecules UC and CeC and Predicted Stability of Diatomic Carbides of Electropositive Transition Metals. *J. Chem. Phys.* **1969**, *50* (5), 2255-2256. DOI: 10.1063/1.1671358.
- (30) Gupta, S. K.; Kingcade, J. E., Jr.; Gingerich, K. A. Experimental and predicted stability of complex gaseous transition metal carbides. *Adv. Mass Spectrom.* **1980**, *8A*, 445-451.
- (31) Kingcade, J. E., Jr.; Cocke, D. L.; Gingerich, K. A. Thermodynamic stabilities of the gaseous cerium carbides CeC, CeC₂, CeC₃, CeC₄, CeC₅, and CeC₆. *High Temp. Sci.* **1983**, *16* (2), 89-109.
- (32) Sevy, A.; Merriles, D. M.; Wentz, R. S.; Morse, M. D. Bond dissociation energies of ScSi, YSi, LaSi, ScC, YC, LaC, CoC, and YCH. *J. Chem. Phys.* **2019**, *151*, 024302. DOI: https://doi.org/10.1063/1.5098330.
- (33) S. Almeida, N. M.; Melin, T. R. L.; North, S. C.; Welch, B. K.; Wilson, A. K. *Ab initio* composite strategies and multireference approaches for lanthanide sulfides and selenides. *J. Chem. Phys.* **2022**, *157* (2), 024105. DOI: https://doi.org/10.1063/5.0094367 (accessed 2022/08/17).
- (34) Kobayashi, M.; Oba, Y.; Akama, T.; Taketsugu, T. Practical electronic ground- and excited-state calculation method for lanthanide complexes based on frozen core potential approximation to 4f electrons. *Journal of Mathematical Chemistry* **2022**. DOI: 10.1007/s10910-022-01356-5.
- (35) McCarver, G. A.; Hinde, R. J.; Vogiatzis, K. D. Selecting Quantum-Chemical Methods for Lanthanide-Containing Molecules: A Balance between Accuracy and Efficiency. *Inorg. Chem.* **2020**, *59* (15), 10492-10500. DOI: 10.1021/acs.inorgchem.0c00808.
- (36) Aebersold, L. E.; Yuwono, S. H.; Schoendorff, G.; Wilson, A. K. Efficacy of Density Functionals and Relativistic Effective Core Potentials for Lanthanide-Containing Species: The Ln54 Molecule Set. *J. Chem. Theory Comput.* **2017**, *13* (6), 2831-2839. DOI: http://dx.doi.org/10.1021/acs.jctc.6b01223 From American Chemical Society . All Rights Reserved. CAPLUS.
- (37) Peterson, C.; Penchoff, D. A.; Wilson, A. K. Ab initio approaches for the determination of heavy element energetics: Ionization energies of trivalent lanthanides (Ln = La-Eu). *J. Chem. Phys.* **2015**, *143* (19), 194109. DOI: http://dx.doi.org/10.1063/1.4935809 From American Chemical Society . All Rights Reserved. CAPLUS.
- (38) Schoendorff, G.; Wilson, A. K. Low valency in lanthanides: A theoretical study of NdF and LuF. *J. Chem. Phys.* **2014**, *140* (22), 224314. DOI: 10.1063/1.4882135 From American Chemical Society . All Rights Reserved. CAPLUS.
- (39) Gingerich, K. A. Stability of rare-earth-containing high-temperature molecules. *J. Less-Common Met.* **1985**, *110*, 41-51.

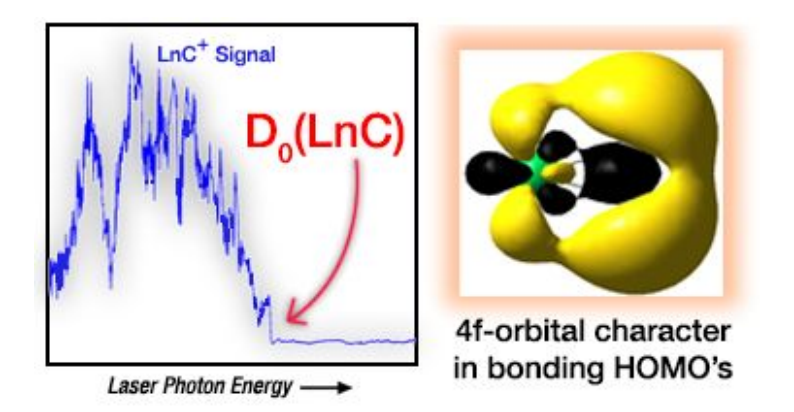
- (40) Grimmel, S.; Schoendorff, G.; Wilson, A. K. Gauging the Performance of Density Functionals for Lanthanide-Containing Molecules. *J. Chem. Theory Comput.* **2016**, *12* (3), 1259-1266. DOI: http://dx.doi.org/10.1021/acs.jctc.5b01193 From American Chemical Society . All Rights Reserved. CAPLUS.
- (41) Pople, J. A. Nobel Lecture: Quantum chemical models. *Rev. Mod. Phys.* **1999**, 71 (5), 1267-1274. DOI: http://dx.doi.org/10.1103/RevModPhys.71.1267.
- (42) Kramida, A.; Ralchenko, Yu.; Reader, J.; and NIST ASD Team (2023), *NIST Atomic Spectra Database (version 5.10)*. [Online]. Available: https://physics.nist.gov/asd [2023, March 7]. National Institute of Standards and Technology, Gaithersburg, MD. DOI: https://doi.org/10.18434/T4W30F.
- (43) Ning, C.; Lu, Y. Electron Affinities of Atoms and Structures of Atomic Negative Ions. *J. Phys. Chem. Ref. Data* **2022**, *51* (2), 021502. DOI: 10.1063/5.0080243 From American Chemical Society . All Rights Reserved. CAPLUS.
- (44) Vitova, T.; Pidchenko, I.; Fellhauer, D.; Bagus, P. S.; Joly, Y.; Pruessmann, T.; Bahl, S.; Gonzalez-Robles, E.; Rothe, J.; Altmaier, M.; et al. The role of the 5f valence orbitals of early actinides in chemical bonding. *Nature Communications* **2017**, *8* (1), 16053. DOI: 10.1038/ncomms16053.
- (45) Neidig, M. L.; Clark, D. L.; Martin, R. L. Covalency in f-element complexes. *Coord. Chem. Rev.* **2013**, *257* (2), 394-406. DOI: https://doi.org/10.1016/j.ccr.2012.04.029.
- (46) Vitova, T.; Roesky, P. W.; Dehnen, S. Open questions on bonding involving lanthanide atoms. *Communications Chemistry* **2022**, *5* (1), 12. DOI: 10.1038/s42004-022-00630-6.
- (47) Minasian, S. G.; Batista, E. R.; Booth, C. H.; Clark, D. L.; Keith, J. M.; Kozimor, S. A.; Lukens, W. W.; Martin, R. L.; Shuh, D. K.; Stieber, S. C. E.; et al. Quantitative Evidence for Lanthanide-Oxygen Orbital Mixing in CeO₂, PrO₂, and TbO₂. *J. Am. Chem. Soc.* **2017**, *139* (49), 18052-18064. DOI: 10.1021/jacs.7b10361.
- (48) Löble, M. W.; Keith, J. M.; Altman, A. B.; Stieber, S. C. E.; Batista, E. R.; Boland, K. S.; Conradson, S. D.; Clark, D. L.; Lezama Pacheco, J.; Kozimor, S. A.; et al. Covalency in Lanthanides. An X-ray Absorption Spectroscopy and Density Functional Theory Study of $LnCl_6^{x-}$ (x = 3, 2). *J. Am. Chem. Soc.* **2015**, *137* (7), 2506-2523. DOI: 10.1021/ja510067v.
- (49) Li, B.; Gu, X.; Jin, P. Overlooked Effects of La-4f Orbitals in Endohedral Metallofullerenes. *Inorg. Chem.* **2022**, *61* (15), 5891-5902. DOI: 10.1021/acs.inorgchem.2c00338.
- (50) Cong, F.; Cheng, J.; Cho, H.-G.; Huang, T.; Wang, X.; Andrews, L. M←NCCH₃, M-η²-(NC)–CH₃, and CN–M–CH₃ Prepared by Reactions of Ce, Sm, Eu, and Lu Atoms with Acetonitrile: Matrix Infrared Spectra and Theoretical Calculations. *Inorg. Chem.* **2021**, *60* (23), 17649-17656. DOI: 10.1021/acs.inorgchem.1c02232.
- (51) Robinson, P. J.; Zhang, X.; McQueen, T.; Bowen, K. H.; Alexandrova, A. N. SmB₆⁻ Cluster Anion: Covalency Involving f Orbitals. *J. Phys. Chem. A* **2017**, *121* (8), 1849-1854. DOI: 10.1021/acs.jpca.7b00247.

- (52) Zhang, W.-J.; Wang, G.-J.; Zhang, P.; Zou, W.; Hu, S.-X. The decisive role of 4f-covalency in the structural direction and oxidation state of XPrO compounds (X: group 13 to 17 elements). *Phys. Chem. Chem. Phys.* **2020**, *22* (47), 27746-27756, 10.1039/D0CP04700G. DOI: 10.1039/D0CP04700G.
- (53) Mooßen, O.; Dolg, M. Two interpretations of the cerocene electronic ground state. *Chem. Phys. Lett.* **2014**, *594*, 47-50. DOI: https://doi.org/10.1016/j.cplett.2014.01.022.
- (54) Shafi, Z.; Gibson, J. K. Lanthanide Complexes Containing a Terminal Ln=O Oxo Bond: Revealing Higher Stability of Tetravalent Praseodymium versus Terbium. *Inorg. Chem.* **2022**, *61* (18), 7075-7087. DOI: 10.1021/acs.inorgchem.2c00525.
- (55) Cheisson, T.; Kersey, K. D.; Mahieu, N.; McSkimming, A.; Gau, M. R.; Carroll, P. J.; Schelter, E. J. Multiple Bonding in Lanthanides and Actinides: Direct Comparison of Covalency in Thorium(IV)- and Cerium(IV)-Imido Complexes. *J. Am. Chem. Soc.* **2019**, *141* (23), 9185-9190. DOI: 10.1021/jacs.9b04061.
- (56) Chen, Z.; Yang, J. Bonding properties of molecular cerium oxides tuned by the 4f-block from *ab initio* perspective. *J. Chem. Phys.* **2022**, *156* (21), 211101. DOI: 10.1063/5.0090214 From American Chemical Society . All Rights Reserved. CAPLUS.
- (57) Sorensen, J. J.; Tieu, E.; Morse, M. D. Bond dissociation energies of lanthanide sulfides and selenides. *J. Chem. Phys.* **2021**, *154*, 124307. DOI: https://doi.org/10.1063/5.0042695.
- (58) Matthew, D. J.; Morse, M. D. Resonant two-photon ionization spectroscopy of jet-cooled UN: Determination of the ground state. *J. Chem. Phys.* **2013**, *138* (18), 184303. DOI: http://dx.doi.org/10.1063/1.4803472 From American Chemical Society . All Rights Reserved. CAPLUS.
- (59) Wiley, W. C.; McLaren, I. H. Time-of-Flight Mass Spectrometer with Improved Resolution. *Rev. Sci. Instrum.* **1955**, *26* (12), 1150 1157.
- (60) Merriles, D. M.; Nielson, C.; Tieu, E.; Morse, M. D. Chemical Bonding and Electronic Structure of the Early Transition Metal Borides: ScB, TiB, VB, YB, ZrB, NbB, LaB, HfB, TaB, and WB. *J. Phys. Chem. A* **2021**, *125* (20), 4420-4434. DOI: https://doi.org/10.1021/acs.jpca.1c02886.
- (61) Merriles, D. M.; Tomchak, K. H.; Ewigleben, J. C.; Morse, M. D. Predissociation measurements of the bond dissociation energies of EuO, TmO, and YbO. *J. Chem. Phys.* **2021**, *155* (14), 144303. DOI: https://doi.org/10.1063/5.0068543 (accessed 2021/10/15).
- (62) Merriles, D. M.; Morse, M. D. Ionization energies and cationic bond dissociation energies of RuB, RhB, OsB, IrB, and PtB. *J. Chem. Phys.* **2022**, *157* (7), 074303. DOI: https://doi.org/10.1063/5.0107086 (accessed 2022/08/17).
- (63) Gaussian 16 Rev. B.01; Wallingford, CT, 2016. (accessed.
- (64) Becke, A. D. Density-functional thermochemistry. III. The role of exact exchange. *J. Chem. Phys.* **1993**, *98* (7), 5648-5652.
- (65) Lu, Q.; Peterson, K. A. Correlation consistent basis sets for lanthanides: The atoms La–Lu. *J. Chem. Phys.* **2016**, *145* (5), 054111. DOI: 10.1063/1.4959280 (accessed 2022/08/29).

- (66) de Jong, W. A.; Harrison, R. J.; Dixon, D. A. Parallel Douglas–Kroll energy and gradients in NWChem: Estimating scalar relativistic effects using Douglas–Kroll contracted basis sets. *J. Chem. Phys.* **2000**, *114* (1), 48-53. DOI: 10.1063/1.1329891 (accessed 2022/08/29).
- (67) Dunning, T. H., Jr. Gaussian basis sets for use in correlated molecular calculations. I. The atoms boron through neon and hydrogen. *J. Chem. Phys.* **1989**, *90* (2), 1007-1023. From American Chemical Society . All Rights Reserved. CAPLUS.
- (68) Kendall, R. A.; Dunning, T. H.; Harrison, R. J. Electron affinities of the first-row atoms revisited. Systematic basis sets and wave functions. *J. Chem. Phys.* **1992**, *96* (9), 6796-6806. DOI: 10.1063/1.462569 (accessed 2021/10/18).
- (69) Douglas, M.; Kroll, N. M. Quantum electrodynamical corrections to the fine structure of helium. *Ann. Phys. (N. Y.)* **1974**, *82* (1), 89-155. DOI: 10.1016/0003-4916(74)90333-9 From American Chemical Society . All Rights Reserved. CAPLUS.
- (70) Hess, B. A. Relativistic electronic-structure calculations employing a two-component no-pair formalism with external-field projection operators. *Phys. Rev. A Gen. Phys.* **1986**, *33* (6), 3742-3748. From American Chemical Society . All Rights Reserved. CAPLUS.
- (71) Jansen, G.; Hess, B. A. Revision of the Douglas-Kroll transformation. *Physical Review A* **1989**, *39* (11), 6016-6017. DOI: 10.1103/PhysRevA.39.6016.
- (72) Merriles, D. M.; Tomchak, K. H.; Nielson, C.; Morse, M. D. Early Transition Metals Strengthen the B₂ Bond in MB₂ Complexes. *J. Am. Chem. Soc.* **2022**, *144* (17), 7557-7561. DOI: https://doi.org/10.1021/jacs.1c13709.
- (73) Cao, X.; Dolg, M. Valence basis sets for relativistic energy-consistent small-core lanthanide pseudopotentials. *J. Chem. Phys.* **2001**, *115* (16), 7348-7355. DOI: 10.1063/1.1406535 From American Chemical Society . All Rights Reserved. CAPLUS.
- (74) Cao, X.; Dolg, M. Segmented contraction scheme for small-core lanthanide pseudopotential basis sets. *J. Mol. Struct. THEOCHEM* **2002**, *581*, 139-147. DOI: 10.1016/s0166-1280(01)00751-5 From American Chemical Society . All Rights Reserved. CAPLUS.
- (75) Pritchard, B. P.; Altarawy, D.; Didier, B.; Gibson, T. D.; Windus, T. L. New Basis Set Exchange: An Open, Up-to-Date Resource for the Molecular Sciences Community. *Journal of Chemical Information and Modeling* **2019**, *59* (11), 4814-4820. DOI: 10.1021/acs.jcim.9b00725.
- (76) Lefebvre-Brion, H.; Field, R. W. Chapter 6 Predissociation. In *Perturbations in the Spectra of Diatomic Molecules*, Lefebvre-Brion, H., Field, R. W. Eds.; Academic Press, 1986; pp 331-382.
- (77) Herzberg, G. *Molecular Spectra and Molecular Structure I. Spectra of Diatomic Molecules*; Van Nostrand Reinhold, 1950.
- (78) Spain, E. M.; Morse, M. D. Bond strengths of transition metal dimers: TiV, V₂, TiCo, and VNi. *J. Phys. Chem.* **1992**, *96*, 2479-2486. DOI: http://dx.doi.org/10.1021/j100185a018.
- (79) Morse, M. D. Predissociation Measurements of Bond Dissociation Energies. *Acc. Chem. Res.* **2019**, 52, 119-126. DOI: http://dx.doi.org/10.1021/acs.accounts.8b00526.

- (80) Spain, E. M.; Morse, M. D. Bond strengths of transition metal diatomics: VNi and V₂. *Int. J. Mass Spectrom. Ion Proc.* **1990**, *102*, 183-197. DOI: http://dx.doi.org/10.1016/0168-1176(90)80059-C.
- (81) Russon, L. M.; Heidecke, S. A.; Birke, M. K.; Conceicao, J.; Armentrout, P. B.; Morse, M. D. The bond strength of Co₂⁺. *Chem. Phys. Lett.* **1993**, *204*, 235-240. DOI: http://dx.doi.org/10.1016/0009-2614(93)90002-I.
- (82) Sorensen, J. J.; Persinger, T. D.; Sevy, A.; Franchina, J. A.; Johnson, E. L.; Morse, M. D. Bond dissociation energies of diatomic transition metal selenides: TiSe, ZrSe, HfSe, VSe, NbSe, and TaSe. *J. Chem. Phys.* **2016**, *145* (21), 214308. DOI: http://dx.doi.org/10.1063/1.4968601.
- (83) Ruscic, B. Active Thermochemical Tables: Sequential Bond Dissociation Enthalpies of Methane, Ethane, and Methanol and the Related Thermochemistry. *J. Phys. Chem. A* **2015**, *119* (28), 7810-7837. DOI: 10.1021/acs.jpca.5b01346 From American Chemical Society . All Rights Reserved. CAPLUS.
- (84) Ghiassee, M.; Stevenson, B. C.; Armentrout, P. B. Evaluation of the $Pr + O \rightarrow PrO^+ + e^-$ cheminonization reaction enthalpy and praseodymium oxide, carbide, dioxide, and carbonyl cation bond energies. *Phys. Chem. Chem. Phys.* **2021**, *23* (4), 2938-2952. DOI: https://pubs.rsc.org/en/content/articlelanding/2021/cp/d0cp06252a From American Chemical Society . All Rights Reserved. CAPLUS.
- (85) Ghiassee, M.; Kim, J.; Armentrout, P. B. Evaluation of the exothermicity of the chemi-ionization reaction Nd + O \rightarrow NdO⁺ + e⁻ and neodymium oxide, carbide, dioxide, and carbonyl cation bond energies. *J. Chem. Phys.* **2019**, *150* (14), 144309. DOI: https://doi.org/10.1063/1.5091679 From American Chemical Society . All Rights Reserved. CAPLUS.
- (86) Hultgren, R.; Desai, P. D.; Hawkins, D. T.; Gleiser, M.; Kelley, K. K.; Wagman, D. D. Selected Values of the Thermodynamic Properties of the Elements; Metals Park, Ohio: American Society for Metals, 1973.
- (87) Ruscic, B.; Bross, D. H. Active Thermochemical Tables (ATcT) values based on Ver. 1.124 of the Thermochemical Network (2022); available at ATcT.anl.gov. 2022. (accessed.
- (88) Sevy, A.; Huffaker, R. F.; Morse, M. D. Bond Dissociation Energies of Tungsten Molecules: WC, WSi, WS, WSe, and WCl. *J. Phys. Chem. A* **2017**, *121* (49), 9446-9457. DOI: http://dx.doi.org/10.1021/acs.jpca.7b09704.
- (89) Sevy, A.; Matthew, D. J.; Morse, M. D. Bond dissociation energies of TiC, ZrC, HfC, ThC, NbC, and TaC. *J. Chem. Phys.* **2018**, *149* (4), 044306. DOI: https://dx.doi.org/10.1063/1.5041422.
- (90) Matthew, D. J.; Tieu, E.; Morse, M. D. Determination of the bond dissociation energies of FeX and NiX (X = C, S, Se). *J. Chem. Phys.* **2017**, *146*, 144310. DOI: http://dx.doi.org/10.1063/1.4979679.
- (91) Johnson, E. L.; Davis, Q. C.; Morse, M. D. Predissociation measurements of bond dissociation energies: VC, VN, and VS. *J. Chem. Phys.* **2016**, *144* (23), 234306. DOI: http://dx.doi.org/10.1063/1.4953782.
- (92) Merriles, D. M.; Tieu, E.; Morse, M. D. Bond dissociation energies of FeB, CoB, NiB, RuB, RhB, OsB, IrB, and PtB. *J. Chem. Phys.* **2019**, *151*, 044302. DOI: https://doi.org/10.1063/1.5113511.

- (93) Desclaux, J. P. Relativistic Dirac-Fock Expectation Values for Atoms with Z=1 to 120. *At. Data Nucl. Data Tables* **1973**, *12*, 311.
- (94) Reed, A. E.; Curtiss, L. A.; Weinhold, F. Intermolecular interactions from a natural bond orbital, donor-acceptor viewpoint. *Chem. Rev.* **1988**, *88* (6), 899-926. DOI: 10.1021/cr00088a005.
- (95) Lu, T.; Chen, F. Multiwfn: A multifunctional wavefunction analyzer. *J. Comput. Chem.* **2012**, *33* (5), 580-592, https://doi.org/10.1002/jcc.22885 (accessed 2021/12/30).
- (96) de Melo, G. F.; Vasiliu, M.; Liu, G.; Ciborowski, S.; Zhu, Z.; Blankenhorn, M.; Harris, R.; Martinez-Martinez, C.; Dipalo, M.; Peterson, K. A.; et al. Theoretical and Experimental Study of the Spectroscopy and Thermochemistry of UC^{+/0/-}. *J. Phys. Chem. A* **2022**, *126* (50), 9392-9407. DOI: 10.1021/acs.jpca.2c06978.
- (97) Hu, S.-X.; Jian, J.; Su, J.; Wu, X.; Li, J.; Zhou, M. Pentavalent lanthanide nitride-oxides: NPrO and NPrO complexes with N≡Pr triple bonds. *Chem. Sci.* **2017**, *8* (5), 4035-4043. DOI: 10.1039/c7sc00710h.
- (98) de Melo, G. F.; Dixon, D. A. Bonding, Thermodynamics, and Spectroscopy of the Metal Borides UB^{0/+/-} and WB^{0/+/-}. *J. Phys. Chem. A* **2023**, *127* (7), 1588-1597. DOI: 10.1021/acs.jpca.2c08556.
- (99) Seitz, M.; Oliver, A. G.; Raymond, K. N. The Lanthanide Contraction Revisited. *J. Am. Chem. Soc.* **2007**, *129* (36), 11153-11160. DOI: 10.1021/ja072750f.
- (100) Barros, N.; Maynau, D.; Maron, L.; Eisenstein, O.; Zi, G.; Andersen, R. A. Single but Stronger UO, Double but Weaker UNMe Bonds: The Tale Told by Cp₂UO and Cp₂UNR. *Organometallics* **2007**, *26* (20), 5059-5065. DOI: 10.1021/om700628e.
- (101) Pyykkö, P. Additive Covalent Radii for Single-, Double-, and Triple-Bonded Molecules and Tetrahedrally Bonded Crystals: A Summary. *J. Phys. Chem. A* **2015**, *119* (11), 2326-2337. DOI: 10.1021/jp5065819.
- (102) Lias, S. G.; Bartmess, J. E.; Liebman, J. F.; Holmes, J. L.; Levin, R. D.; Mallard, W. G. Gas-phase ion and neutral thermochemistry. *J. Phys. Chem. Ref. Data, Suppl.* **1988**, *17* (1), 861 pp. From American Chemical Society . All Rights Reserved. CAPLUS.
- (103) Li, X.; Wang, L.-S. Electronic structure and chemical bonding between the first row transition metals and C₂: A photoelectron spectroscopy study of MC₂⁻ (M=Sc, V, Cr, Mn, Fe, and Co). *J. Chem. Phys.* **1999**, *111* (18), 8389-8395.
- (104) Filby, E. E.; Ames, L. L. Dissociation energies for gaseous metal dicarbides. *Inorganic and Nuclear Chemistry Letters* **1972**, *8* (10), 855-860.
- (105) Gibson, J. K. Chemistry of actinide and lanthanide metal ions (M⁺) in laser ablation of dispersions of inorganic compounds in polyimide and polytetrafluoroethylene. *Journal of Vacuum Science & Technology, A: Vacuum, Surfaces, and Films* **1997**, *15* (4), 2107-2118. DOI: 10.1116/1.580616 From American Chemical Society . All Rights Reserved. CAPLUS.
- (106) Luo, Y.-R. *Comprehensive Handbook of Chemical Bond Energies*; CRC Press, Taylor and Francis Group, 2007. DOI: 10.1201/9781420007282.



TOC Graphic

Synopsis

The figure on the left illustrates how the observation of a sharp predissociation threshold is used to measure the bond dissociation energies of the LnC and Tm- C_2 molecules. The figure on the right illustrates 4f orbital character on Tm combining with the $2\sigma_g$ orbital of C_2 , leading to the transfer of electron density into the otherwise vacant $2\sigma_g$ bonding orbital of the C_2 unit.